

HIGH-ORDER HARMONIC GENERATION IN LASER-IRRADIATED HOMONUCLEAR DIATOMICS: THE VELOCITY GAUGE VERSION OF MOLECULAR STRONG-FIELD APPROXIMATION

Vladimir I. Usachenko^{1,2,3}, Pavel E. Pyak² and Shih-I Chu⁴

¹*Institute of Applied Laser Physics UzAS, Katartal str. 28, Tashkent, 100135, Uzbekistan,*

²*Physics Department, National University of Uzbekistan, Tashkent, 100174, Uzbekistan*

³*Max-Born-Institute for Nonlinear Optics and Short-Pulse Laser Spectroscopy,
Berlin, 12489, Germany*

⁴*Department of Chemistry, University of Kansas, Lawrence, KS 66045-7582, USA*

The generation of high harmonics in laser-irradiated light homonuclear diatomics (H_2^+ , N_2 and O_2) compared to that in atomic counterparts (of nearly identical binding energy) is studied within the *velocity gauge* version of conventional *strong-field approximation*. The applied strong-field approach (alternatively developed earlier to incorporate rescattering effects beyond the conventional saddle-point approximation) is currently extended to molecular case by means of supplement the standard *linear combination of atomic orbitals* and *molecular orbitals* method. The associated model proved to adequately reproduce a general shape and detailed structure of molecular harmonic spectra, which demonstrate a number of remarkable distinctive differences from respective atomic spectra calculated under the same laser pulses. The revealed differences are found to be strongly dependent on internuclear separation and also very sensitive to the orbital and bonding symmetry of contributing molecular valence shell. In particular, the model correctly predicts the behavior of high-frequency plateau (both for its extent and even details of structure) in molecular harmonic spectra at small (nearly equilibrium) and large internuclear separations. In addition, for some group of harmonics, the harmonic emission rates were ascertained to dominate by contribution from inner molecular shells of higher binding energy and different orbital symmetry compared to the outermost molecular orbital normally predominantly contributing.

¹*Corresponding author, permanent mailing address: Institute of Applied Laser Physics UzAS, Katartal str., 28, Tashkent, 700135, Uzbekistan. E-mail: vusach@yahoo.com.*

HIGH-ORDER HARMONIC GENERATION IN LASER-IRRADIATED HOMONUCLEAR DIATOMICS: THE VELOCITY GAUGE VERSION OF MOLECULAR STRONG-FIELD APPROXIMATION

Vladimir I. Usachenko^{1,2,3}, Pavel E. Pyak² and Shih-I Chu⁴

¹*Institute of Applied Laser Physics UzAS, Katartal str. 28, Tashkent, 100135, Uzbekistan,*

²*Physics Department, National University of Uzbekistan, Tashkent, 100174, Uzbekistan*

³*Max-Born-Institute for Nonlinear Optics and Short-Pulse Laser Spectroscopy,
Berlin, 12489, Germany*

⁴*Department of Chemistry, University of Kansas, Lawrence, KS 66045-7582, USA*

1. INTRODUCTION AND BACKGROUND MOTIVATION.

Apart from pure fundamental interest, the strong-field phenomenon of high-order harmonic generation (HHG) in laser-irradiated species is currently believed to be a highly promising for creation compact (table-top) sources of ultra-short (sub-femtosecond) pulses of powerful coherent XUV radiation [1, 2]. Being accessible, such a high-frequency radiation might be used for X-ray holography or monitoring of biological processes *in vivo* [2] as well as tomographic imaging of molecular orbitals [3] with an unprecedented brightness and spatial and temporal resolution. For the reasons above, the HHG process became a subject of equally great experimental and theoretical interest in the last decade (see also e.g., [4-6], for review and references cited therein). Compared to atoms, the laser-irradiated molecules as sources of high harmonics [7-14] offer promising prospects as to raising the up to now disappointingly low conversion efficiency for harmonic generation [7-12] and/or harmonic cutoff frequency [10, 13] due to an advanced possibility of controlling and manipulating the additional external degrees of freedom in molecules. For example, the internuclear distance R_0 of simplest diatomic molecules, which determines differently delocalized initial electronic states, can be used to enhance the harmonic conversion efficiency exceeding the atomic one due to transient enhancement of harmonic emission in expanding molecules [12]. Particularly, the calculated harmonic conversion efficiency was found to be noticeably enhanced (by several orders of magnitude) with increasing of R_0 over equilibrium internuclear separation [10, 12, 14]. Diatomic molecules may also produce high harmonics of much higher cutoff frequency due to a much longer high-frequency plateau extended up to $8U_p$ of maximum length [10] versus the respective maximum value $3.17U_p$ ascertained for atomic harmonic spectra (here U_p is the ponderomotive energy of field-induced oscillating motion of an electron in the continuum; the *atomic system of units* is used unless stated otherwise).

Because of the electron wavelength is comparable to the size of the molecular wavefunction, the intensity of emission at a particular X-ray photon energy is also expected to be sensitive to the wavelength of the electron wave and the shape of the molecular wavefunction and/or orientation of internuclear molecular axis with respect to incident laser field polarization [8-11]. In addition, simultaneous observation of both ion yields and harmonic signals [15] under the same conditions was shown to serve as an effective tool

¹*Corresponding author, permanent mailing address: Institute of Applied Laser Physics UzAS, Katartal str., 28, Tashkent, 700135, Uzbekistan. E-mail: vusach@yahoo.com.*

to probe molecular structure in an instant [16] and also make it possible to use quantum phenomena in HHG associated with molecular symmetries to disentangle the contributions from the ionization and recombination processes [17]. In this context, homonuclear (or homopolar) diatomics seem to be also of special interest due to identical atomic nuclei give rise to a possibility of various laser field-induced and orientation-dependent *intramolecular interference* effects [15] that may additionally affect the molecular HHG process. The clear signs of intramolecular interference-related effects due to two-centered nature of diatomic molecule were numerically revealed [11] in high-harmonic spectra of model (1D or 2D) H_2^+ and H_2 systems as a broad and pronounced local minimum of the position strongly dependent on the internuclear separation and spatial orientation of diatomic molecule. The origin of the minimum was attributed to the *destructive* interference of photoelectron emission from separate atomic centers [11], so that a transparent interpretation can be given in terms of interference between two radiating point sources located at the positions of the nuclei. The latter pivotal idea (obviously proposed first in Ref. [18]) about intramolecular interference of atomic photoionization amplitudes was successfully exploited in [19] for description of molecular ionization as compared to ionization of respective atomic counterparts having nearly identical binding energies. Based on the *velocity gauge* formulation of conventional *strong-field approximation* (SFA) (see, e.g. [20] and associated *Keldysh-Faisal-Reiss* theories [21]) with the atomic ionization rates modified by the interference from the atomic centers, the molecular ionization was predicted to be enhanced (or, at least, not suppressed) in N_2 (versus Ar) and/or suppressed in O_2 (versus Xe). The mentioned suppression in O_2 was interpreted in terms of the strong-field MO-SFA model [19] as intimately related to intramolecular interference, which is to be always destructive for low-energy photoelectrons emitted from the $1\pi_g$ *highest-occupied molecular orbital* (HOMO) of *antibonding* symmetry and predominantly contributing to respective ionization rate. Accordingly, the background physical mechanism underlying an enhanced ionization in N_2 versus Ar was identified as constructive intramolecular interference for low-energy photoelectrons emitted from the $3\sigma_g$ HOMO in N_2 of *bonding* symmetry.

Meantime, because of the high suppression in strong-field ionization of O_2 versus Xe , the laser-irradiated diatomic O_2 is expected to produce high harmonics of noticeably higher *cutoff* frequency as compared to Xe atom [13]. Namely, due to a suppressed molecular ionization in H_2 and O_2 (versus their atomic counterparts) and correspondingly larger value of the saturation intensity, the latter diatomics survive at a considerably higher laser intensity (at which their atomic counterparts are to be completely ionized) and, thus, they are still able to produce harmonics of a considerably higher *cutoff* frequency (proportional to laser intensity). The related extension of high-frequency plateau in harmonic spectra of O_2 relative to Xe , was recently observed in experiment and numerically simulated [13] based on the Lewenstein model [22] supplemented by the molecular tunneling ionization (or the so-called MO-ADK) theory [23] to account for the differences in ionization of molecules compared to atoms in terms of *Ammosov-Delone-Krainov* (ADK) model of tunneling ionization [24]. The MO-ADK model partly succeeded in reproducing of suppressed ionization (e.g., in O_2 versus Xe compatible with experiment [25]), although, being applied to molecular HHG, the model seems to encounter difficulties in providing a transparent interpretation and satisfactory agreement with experiment in prediction of the *cutoff* frequency observed in molecular high-harmonic spectra [13] (see also Sec.4 below, for details). Being also applied to ionization of other diatomic species (e.g., in H_2 versus companion Ar atom), the ADK-based approach resulted in a dis-

crepancy with experiment [26], at least in the strong-field domain (i.e., only where the tunneling theory is generally valid). Since the wavefunction of initial molecular state corresponding to HOMO is always approximated by only a *single one-centered* atomic orbital within the MO-ADK model, such theory is not suitable either for adequate description of intramolecular interference-related phenomena arising from the *two-centered* nature of molecular valence shell in diatomics.

Thus, there are numerous interrelated and remarkable aspects of molecular HHG and above-threshold ionization (ATI) as a prerequisite to the HHG, which appear to be also strongly interdependent and interrelated in laser-irradiated molecules too. However, with the possible few exceptions, the fundamental physics associated with how atoms and molecules respond to intense laser radiation (i.e. optical fields approaching the atomic unit) cannot be treated exactly due to the comparable strengths of the electron-nucleus, electron-electron and electron-field interaction. Although *ab initio* quantum calculations for atoms are readily available, at least within the *single-active electron* (SAE) approximation, this is not the case for molecules as fully three-dimensional (3D) calculations on even relatively simple diatomics, such as H_2^+ , are extremely difficult [14]. Therefore, the HHG process in diatomic molecules is primarily treated nowadays using approximate SAE-based general strong-field approaches, such as conventional *strong-field approximation* (SFA) formulated in terms of "rescattering" (or recollision) picture and model zero-range binding potential of atomic centers [10] and/or various pure numerical procedures (see e.g. [27]) and simulations (e.g., [8, 11, 12]). The harmonic emission rates for molecules can be also calculated, in principle, based on different *ab initio* numerical procedures and methods, such as direct numerical solution of time-dependent Schrödinger equation (TDSE method, e.g., [11]) and time-dependent density-functional theory (TD-DFT) including many-electron effects [28]; however, the related results seem to be very computationally demanding and hardly available for reliable and transparent interpretation.

All the aspects above gave us a strong motivation to consider the harmonic generation in laser-irradiated diatomics and verify the mentioned aspects within the currently proposed alternative model of molecular HHG. The model is based on fully quantum-mechanical SAE-based strong-field approach developed earlier [29, 30] and proved to adequately incorporate rescattering effects in atomic HHG and high-energy ATI processes. In the present paper the proposed strong-field approach is extended to molecular case of diatomic specie (i.e. substantially many-electron system) by means of supplement the standard *linear combination of atomic orbitals* (LCAO) and *molecular orbitals* (MO) method invoked for approximate reproducing the two-centered one-electron wavefunction of initial molecular discrete state. The LCAO-MO method proved to be surprisingly well working for adequate description and transparent interpretation the phenomena of enhanced (and/or suppressed) ionization of laser-irradiated diatomics in terms of previously developed strong-field SFA-LCAO model [31]. This model is to be also used further in Sec.3 for numerical calculation and evaluation of laser intensity for ionization saturation under conditions of molecular HHG experiment [13]. The related results for calculated harmonic emission rates (or high-harmonic conversion efficiency) and position of high-frequency plateau cutoff proved to be sensitive to the molecular orbital symmetry and internuclear separation. At last, our present consideration is not restricted to only one, a single (the outermost) molecular valence shell, so that other (inner) contributing molecular orbitals of higher binding energies and different orbital symmetry are additionally and equally well incorporated, wherever appropriate. The proposed molecular HHG model is shown to adequately reproduce the distinctive features of molecular harmonic

spectra compared to respective atomic spectra as well as noticeable differences found in structure of molecular harmonic spectra corresponding to HOMO of bonding symmetry (e.g., $3\sigma_g$ in N_2) relative to antibonding symmetry (e.g., $1\pi_g$ in O_2).

2. THE APPLIED STRONG-FIELD HHG MODEL: BASIC ASSUMPTIONS AND ANALYTICAL RELATIONS.

The harmonic emission process under discussion is to be further investigated within framework of the strong-field fully quantum-mechanical approach developed in [29, 30] and applied previously to treatment of atomic HHG process. Let's outline first in brief the main features of related strong-field model, which is currently to be extended to molecular case. Within the *dipole approximation* (neglecting any photon momenta) the Hamiltonian of EM interaction in the *velocity gauge* (VG) form, reads as

$$\widehat{W}(\mathbf{r}, t) = \frac{1}{c_0} \mathbf{A}(t) \cdot \widehat{\mathbf{p}} + \frac{1}{2c_0^2} \mathbf{A}^2(t) \quad (1)$$

where $\widehat{\mathbf{p}} = -i\nabla$ is the operator of electron canonical momentum, $c_0 \approx 137$ is the light velocity in vacuum. This means that the vector potential $\mathbf{A}(t)$ of incident laser field and associated field strength $\mathbf{E}(t)$ are supposed to be independent on coordinate \mathbf{r} , but both are functions of time t only. Our present consideration will be restricted entirely to the case of only harmonic emission processes in which the atomic or molecular specie occupies the same state before and after the passage of the laser pulse. Thus, the bound discrete state is supposed to be unperturbed by incident laser field and the respective undistorted (laser-free) stationary wavefunction $\Phi_0(\mathbf{r}, t) = \Phi_0(\mathbf{r}) \exp(-i\varepsilon_0 t)$ already known in advance (or, at least, found to any arbitrary prescribed accuracy).

Then, for particular case of linearly polarized laser field of the frequency ω , electric field strength E and unit polarization vector \mathbf{e} :

$$\mathbf{A}_L(t) = (c_0/\omega) \mathbf{e} E \cos(\omega t) \quad (2)$$

the total SFA-amplitude of HHG can be expressed through the sum of partial amplitudes $f_N^{(HHG)}(\Omega_{\mathbf{k}'})$ of emission of high-harmonic of N -th order, frequency $\Omega_{\mathbf{k}'}$ and polarization $\mathbf{e}_{\mathbf{k}', \lambda}$ ($\lambda = 1, 2$):

$$\begin{aligned} f_{i \rightarrow f}^{(HHG)}(\Omega_{\mathbf{k}'}) &= \sum_N f_N^{(HHG)}(\Omega_{\mathbf{k}'}) \delta(\Omega_{\mathbf{k}'} - N\omega) = \\ &= -\sqrt{\frac{2\pi}{V\Omega_{\mathbf{k}'}}} \int_{-\infty}^{\infty} Q_\Omega(t) \exp(i\Omega_{\mathbf{k}'} t) dt \end{aligned} \quad (3)$$

where

$$Q_\Omega(t) = i\Omega_{\mathbf{k}'} D_\Omega(t) = i\Omega_{\mathbf{k}'} \sum_N \widetilde{D}_\Omega^{(N)}(\omega) \exp(-iN\omega t) \quad (4)$$

with the time-dependent dipole moment $D_\Omega(t)$ induced in a laser-irradiated system by incident laser field, whereas V is the spatial normalization volume. The N -th Fourier component $\widetilde{D}_\Omega^{(N)}(\omega)$ of the field-induced dipole moment can be derived in the following analytical form [29]:

$$\begin{aligned} \widetilde{D}_\Omega^{(N)}(\omega) &= \sum_{m \geq N_0} R_{N-m, m}(\Omega_{\mathbf{k}'}, q_m, \eta) = -i\pi\Omega_{\mathbf{k}'}^{-1} \sum_{m \geq N_0} (U_p - m\omega) \times \\ &\times q_m \int (\mathbf{e}_{\mathbf{k}', \lambda}^* \cdot \mathbf{q}_m) B_{N-m}\left(\zeta(\mathbf{q}_m); \frac{\eta}{2}\right) B_{-m}\left(\zeta(\mathbf{q}_m); \frac{\eta}{2}\right) |F_0(\mathbf{q}_m)|^2 dO_{\mathbf{q}_m} \end{aligned} \quad (5)$$

Here

$$F_0(\mathbf{q}) \equiv (2\pi)^{-3/2} \int d\mathbf{r} \cdot \exp(-i\mathbf{q} \cdot \mathbf{r}) \Phi_0(\mathbf{r}) \quad (6)$$

is the Fourier transform of stationary wavefunction $\Phi_0(\mathbf{r})$ of laser-exposed specie corresponding to initial bound discrete state unperturbed by incident laser field, while $B_s(x; y)$ is the s -th order generalized Bessel function [20] of two real arguments as dimensionless parameters:

$$\zeta(\mathbf{p}) = (\mathbf{E} \cdot \mathbf{p}) / \omega^2, \quad \eta = U_p / \omega = E^2 / (4\omega^3) \quad (7)$$

with ponderomotive energy U_p of field-induced oscillating motion of electron driven in continuum. The variable $q_m = \sqrt{2(m\omega - I_p - U_p)}$ in Eq.(5) denotes discrete values of photoelectron canonical momentum in intermediate continuum states of energies

$$\varepsilon_{\mathbf{q}}^{(m)} = m\omega - I_p - U_p \quad (8)$$

corresponding to m number of absorbed laser photons beginning from the minimum one $N_0 \equiv N_0(\eta) = [(I_p + U_p) / \omega] + 1$ required for ionization (here $[x]$ denotes an integer part of variable x).

Due to the "pole approximation" applied, the summation in (5) over positive integer $m \geq N_0$ takes into account the resonance (or "essential") intermediate continuum states corresponding to open ATI channels (to which the process of direct ATI is also possible), which are only supposed to give the main (predominant) contribution to HHG process under consideration (see also [29] for details). It is also worth noting that the time-independent matrix function $R_{n,m}(\Omega_{\mathbf{k}'}, q_m, \eta)$ allows for representation in the factorized form:

$$R_{n,m}(\Omega_{\mathbf{k}'}, q_m, \eta) = \int f_n^{(SR)}(\Omega_{\mathbf{k}'}, \mathbf{q}_m, \eta) f_m^{(MPI)}(\mathbf{q}_m, \eta) dO_{\mathbf{q}_m} \quad (9)$$

that makes the final results transparent for interpretation. Namely, the integrand in (9) is a product of time-independent amplitudes of two strong-field multiphoton processes - the direct ATI process accompanied by absorption of m incident laser photons and emission of a photoelectron to intermediate continuum states of canonical momentum \mathbf{q}_m

$$f_m^{(MPI)}(\mathbf{q}_m, \eta) \sim 2\pi (U_p - m\omega) B_{-m}\left(\zeta(\mathbf{q}_m); \frac{\eta}{2}\right) F_0(\mathbf{q}_m) \quad (10)$$

followed by subsequent process of spontaneous photorecombination and emission of a high-harmonic photon of frequency $\Omega_{\mathbf{k}'}$ and polarization $\mathbf{e}_{\mathbf{k}',\lambda'}$ ($\lambda = 1, 2$):

$$f_n^{(SR)}(\Omega_{\mathbf{k}'}, \mathbf{q}_m, \eta) \sim iq_m \sqrt{2\pi/\Omega_{\mathbf{k}'}^3} (\mathbf{e}_{\mathbf{k}',\lambda'}^* \cdot \mathbf{q}_m) B_n\left(\zeta(\mathbf{q}_m); \frac{\eta}{2}\right) F_0^*(\mathbf{q}_m) \quad (11)$$

Finally, the high-harmonic spectrum within the proposed model is represented by a sequence of equidistant (separated by a laser fundamental frequency ω) discrete peaks of heights defined by the partial HHG amplitudes $f_N^{(HHG)}(\Omega_{\mathbf{k}'})$ (3) and respective differential rates $w_N^{(HHG)}(\mathbf{k}')$:

$$w_N^{(HHG)}(\mathbf{k}') = \frac{\Omega_N^3}{(2\pi c_0)^3} \left| \widetilde{D}_{\Omega_N}^{(N)}(\omega) \right|^2 \quad (12)$$

of emission of high-harmonic photon of discrete frequency $\Omega_N = N\omega$ to a fixed solid angle element $dO_{\mathbf{k}'}$.

The total ionization rates $\Gamma_{ion}(\eta)$ can be derived just from the amplitude (10) of direct ATI process by means of integration of its squared modulus over the angles of

photoelectron emission as well as photoelectron energy. The integration over the final energy of emitted photoelectron is just reduced to the summation over the total number N of laser photons absorbed (see, also [30, 31], for details):

$$\Gamma_{ion}(\eta) = \sum_{N \geq N_0(\eta)} \frac{p_N}{(2\pi)} (U_p - N\omega)^2 \int dO_{\mathbf{p}_N} B_{-N}^2 \left(\zeta(\mathbf{p}_N); \frac{\eta}{2} \right) |F_0(\mathbf{p}_N)|^2 \quad (13)$$

In a pulsed laser field of arbitrary duration τ , the total yield of photoelectrons (i.e., the produced photoelectron and/or ion signal that is measured in experiment) depends on the peak field strength E_0 and laser's spatial and temporal profiles. For spatially homogeneous incident laser field, the amplitude E of laser field is only dependent on the peak field strength E_0 and temporal profile function $g(t)$ according to:

$$\mathbf{E}(t) = \mathbf{e}E(t) \sin(\omega t) = \mathbf{e}E_0 g(t) \sin(\omega t) \quad (14)$$

So, for example, for *Gaussian* shape of laser pulse intensity:

$$g(t) = \exp \left[-2 \left(\frac{t - t_0}{\tau} \right)^2 \ln 2 \right] \quad (15)$$

with $t_0 = \tau/2$ as the time moment at which the laser intensity reaches a maximum during the laser pulse duration. Under conventional supposition that the ionization process is generally a considerably faster than the time period of essential change of temporal profile function $g(t)$, the ionization rate (13) derived assuming time-independent laser field intensity can be approximately considered as still valid, but corresponding to the instant ionization rate. This means that the ionization rate (13) is just supposed to be adiabatically changing with variation of laser intensity through the laser pulse action and the total ionization probability for the overall time of laser pulse duration τ can be found according to the quasistatic formula:

$$P_{ion}(\tau) = 1 - \exp \left(- \int_0^\tau \Gamma_{ion}(\eta(t)) dt \right) \quad (16)$$

where, particularly

$$\eta(t) = E^2(t) / (4\omega^3) = g^2(t) E_0^2 / (4\omega^3) \quad (17)$$

The Eq.(16) will be used further for defining the saturation ionization intensity I_{sat} as the laser intensity which leads to 99% of the laser-irradiated species being ionized by the ending time of the laser pulse, so that $P_{ion}(\tau) \approx 0.99$.

3. SAE-EXTENSION TO MOLECULAR HHG IN DIATOMIC MOLECULES: THE MOLECULAR ORBITALS IN COORDINATE AND MOMENTUM SPACE.

So far, up to this point, we didn't specify the nature of laser-irradiated system, so that all the relations above are supposed to be equally well applicable to arbitrary atomic and/or molecular species provided the SAE consideration is valid to derive the Fourier transform of a single-electron wavefunction of initial bound discrete state in a closed analytical form. Thus, according to the HHG model currently extended to molecular case of homonuclear diatomics, the specified properties of laser-irradiated system are incorporated solely through the ionization potential $I_p^{(n)}$ and Fourier transform (6) being the wavefunction $F_n(\mathbf{p}; \mathbf{R}_0)$ of initial n -th molecular discrete state in momentum space. The corresponding single-electron wavefunctions, or *molecular orbitals*, each of a fixed

discrete binding energy $\varepsilon_0^{(n)} = -I_p^{(n)}$ and respective number $N_e^{(n)}$ of identical electrons, are the mathematical constructs used to describe the multi-electron wavefunction in molecules (similar to *atomic orbitals* in atom). According to the standard linear combination of atomic orbitals (LCAO) and molecular orbitals (MO) method, the wavefunction of each (n -th) molecular valence shell can be approximately considered as *two-centered* MO:

$$\begin{aligned} \Phi_n(\mathbf{r}_1; \mathbf{r}_2) &= \Phi_n(\mathbf{r} - \mathbf{R}_0/2; \mathbf{r} + \mathbf{R}_0/2) = \\ &= \sum_j \sqrt{\frac{N_e^{(n)}}{2(1 \pm S_j^{(n)}(R_0))}} \left[\phi_j^{(n)}(\mathbf{r} - \mathbf{R}_0/2) \pm \phi_j^{(n)}(\mathbf{r} + \mathbf{R}_0/2) \right] \end{aligned} \quad (18)$$

being a linear superposition of predominantly contributing (j -th) *one-electron* AOs $\phi_j^{(n)}(\mathbf{r})$ centered on each of the atomic cores and thus separated by internuclear distance R_0 . Here

$$S_j^{(n)}(R_0) = \int d\mathbf{r} \phi_j^{(n)}(\mathbf{r} + \mathbf{R}_0/2) \phi_j^{(n)}(\mathbf{r} - \mathbf{R}_0/2) \quad (19)$$

is the respective atomic orbital overlap integral.

Because the highest-lying orbitals are responsible for chemical properties, they are of particular interest. For N_2 molecule and the $3\sigma_g$ HOMO of gerade and bonding symmetry commonly considered, the approximate two-centered single-electron molecular wavefunction can be composed, for example, as a superposition of scaled hydrogen-like $2p_z$ or $1s$ atomic orbitals [31]:

$$\Phi_{(2p)3\sigma_g}(\mathbf{r}; \mathbf{R}_0) = \sqrt{\frac{N_e^{(3\sigma_g)}}{2(1 - S_{2p_z}^{(3\sigma_g)}(R_0))}} \left[\phi_{2p_z}^{(3\sigma_g)}(\mathbf{r} - \mathbf{R}_0/2) - \phi_{2p_z}^{(3\sigma_g)}(\mathbf{r} + \mathbf{R}_0/2) \right] \quad (20)$$

$$\Phi_{(1s)3\sigma_g}(\mathbf{r}; \mathbf{R}_0) = \sqrt{\frac{N_e^{(3\sigma_g)}}{2(1 + S_{1s}^{(3\sigma_g)}(R_0))}} \left[\phi_{1s}^{(3\sigma_g)}(\mathbf{r} - \mathbf{R}_0/2) + \phi_{1s}^{(3\sigma_g)}(\mathbf{r} + \mathbf{R}_0/2) \right] \quad (21)$$

Accordingly, for ungerade $1\pi_u$ inner valence shell of bonding symmetry or gerade $1\pi_g$ HOMO of antibonding symmetry commonly considered in O_2 molecule, the respective approximate two-centered single-electron molecular wavefunction can be composed, for example, as a superposition of scaled hydrogen-like $2p_x$ (or $2p_y$) atomic orbitals [31]:

$$\Phi_{(2p)1\pi_u}(\mathbf{r}; \mathbf{R}_0) = \sqrt{\frac{N_e^{(1\pi_u)}}{2(1 + S_{2p_x}^{(1\pi_u)}(R_0))}} \left[\phi_{2p_x}^{(1\pi_u)}(\mathbf{r} - \mathbf{R}_0/2) + \phi_{2p_x}^{(1\pi_u)}(\mathbf{r} + \mathbf{R}_0/2) \right] \quad (22)$$

$$\Phi_{(2p)1\pi_g}(\mathbf{r}; \mathbf{R}_0) = \sqrt{\frac{N_e^{(1\pi_g)}}{2(1 - S_{2p_x}^{(1\pi_g)}(R_0))}} \left[\phi_{2p_x}^{(1\pi_g)}(\mathbf{r} - \mathbf{R}_0/2) - \phi_{2p_x}^{(1\pi_g)}(\mathbf{r} + \mathbf{R}_0/2) \right] \quad (23)$$

Note first that the “-” combination in the right-hand side of Eq.(18) doesn’t not necessarily correspond to an *antibonding* valence shell (such as π_g or σ_u) having a negligibly small electron density near the central region between the atomic nuclei in homonuclear diatomic. Neither the sign “+” always corresponds to a *bonding* valence shell only (such as σ_g or π_u) with a considerable electron density near the internuclear axis region. Let us also recall, that the “+” superposition of contributing AOs doesn’t not necessarily imply only *gerade* (viz. spatially symmetric, like σ_g or π_g) molecular valence shells, but it may

be also inherent to *ungerade* (viz. antisymmetric, like, e.g. π_u) bonding MOs. Accordingly, the "–" superposition may also correspond both to *gerade* (such as antibonding π_g) and *ungerade* (such as bonding π_u) molecular valence shells. Thus, depending on the spatial parity of contributing AOs $\phi_j^{(n)}(\mathbf{r})$, the "+" or "–" combination in the right-hand side of (18) is chosen to provide a required spatial and bonding symmetry of composed molecular valence shell. Meantime, the form of contributing AOs $\phi_j^{(n)}(\mathbf{r})$ in (20)-(23) is generally chosen to adequately (although, approximately) reproduce the spatial distribution of electronic density in respective MO under consideration relative to the internuclear axis. In particular, an appropriate choice of predominantly contributing AOs $\phi_j^{(n)}(\mathbf{r})$ allows for approximate reproducing a considerable electron density (inherent to σ valence shells) or negligibly small electron density (inherent to π valence shells) nearly along the internuclear axis spatial region, irrespectively of bonding or antibonding symmetry. For example, the $3\sigma_g$ HOMO in N_2 is well-known as a considerably prolate along the internuclear axis, so that respective spatial distribution of molecular electron density can be approximately reproduced by the linear combination (20) of two predominantly contributing $2p_z$ hydrogen-like atomic orbitals, which are oriented along the internuclear molecular axis (supposed to be coincident with spatial OZ axis). Accordingly, the $1\pi_g$ HOMO in O_2 is well-known to have a negligible electron density along the internuclear axis and this feature can be adequately reproduced by a single linear combination (23) of two predominantly contributing $2p_x$ (or $2p_y$) scaled hydrogen-like atomic orbitals, which are oriented perpendicularly to the internuclear axis.

We have to mention here that the "+" combination of $2p_z$ scaled hydrogen-like atomic orbitals we previously used in [31] to reproduce $3\sigma_g$ HOMO in N_2 doesn't provide the even (*gerade*) spatial parity and *bonding* symmetry of the $(2p)3\sigma_g$, although proved to be a surprisingly well working in explaining of relevant experiment [26] (which, particularly, shows no suppression found in strong-field ionization of N_2). Therefore, presently the "–" combination of $2p_z$ states in Eq.(20) is used, which does provide the even spatial parity of the $(2p)3\sigma_g$ HOMO. However, according to the MO-SFA model [19], such a composition would result in destructive intramolecular interference and accordingly high suppression in ionization of N_2 (see also [31], for details). To eliminate the mentioned deficiency, in our present consideration we apply a more accurate composition of the $3\sigma_g$ HOMO taking into account some admixture of contribution from atomic *s*-states required mostly to provide a good agreement with experiment (which doesn't show a suppressed ionization in N_2). Thus, the $3\sigma_g$ MO is to be further approximated by the *coherent superposition* of few different MOs corresponding to separate contributions from atomic states of a specified orbital symmetry (viz., the scaled hydrogen-like $1s$, $2s$ and $2p_z$ orbitals):

$$\Phi_{(1s2s2p)3\sigma_g}(\mathbf{r}; \mathbf{R}_0) = A_{1s}\Phi_{(1s)3\sigma_g}(\mathbf{r}; \mathbf{R}_0) + A_{2s}\Phi_{(2s)3\sigma_g}(\mathbf{r}; \mathbf{R}_0) + A_{2p}\Phi_{(2p)3\sigma_g}(\mathbf{r}; \mathbf{R}_0) \quad (24)$$

with the weight coefficients A_j ($j = 1, 2, 3$) being the relative contributions ($|A_j| \leq 1$) from respective atomic states and considered as variational parameters to be found from the equation for minimum of respective molecular binding energy, the value of which is put to be equal to the experimental value. Unlike this, the $1\pi_g$ HOMO in O_2 is further supposed to be reproduced by the single $(2p)1\pi_g$ MO (24), which proved to be fairly well working [31] in interpretation of a high suppression of strong-field ionization found in relevant experiment [25, 26].

The applied velocity gauge (VG) formulation of SFA consideration of molecular strong-field ionization also implies analytical representation for Fourier transform $F_n(\mathbf{q}, \mathbf{R}_0)$ corresponding to matrix element (6) of EM transition from the n -th initial molecular

discrete state $\Phi_n(\mathbf{r}; \mathbf{R}_0)$ to the final continuum state of a definite value of canonical momentum \mathbf{p} . For molecular valence shells $3\sigma_g$ in N_2 and $1\pi_g$ in O_2 under consideration, the explicit expressions (20)-(23) allow for direct analytical calculation of respective Fourier transform (or molecular wavefunction in momentum space) for each of contributing one-electron two-centered single molecular orbitals:

$$F_{(2p)3\sigma_g}(\mathbf{p}_N, \mathbf{R}_0) = -\sqrt{N_e^{(3\sigma_g)}} C(\kappa_n) \frac{2^5 \kappa_n^{7/2} p_N \cos(\theta_{\mathbf{p}})}{\pi \sqrt{2} (p_N^2 + \kappa_n^2)^3} \frac{\sin[(\mathbf{p}_N \cdot \mathbf{R}_0)/2]}{\sqrt{2[1 - S_{2p_z}(R_0)]}} \quad (25)$$

$$F_{(2s)3\sigma_g}(\mathbf{p}_N, \mathbf{R}_0) = \sqrt{N_e^{(3\sigma_g)}} C(\kappa_n) \frac{2^4 \kappa_n^{5/2} (p_N^2 - \kappa_n^2)}{\pi \sqrt{2} (p_N^2 + \kappa_n^2)^3} \frac{\cos[(\mathbf{p}_N \cdot \mathbf{R}_0)/2]}{\sqrt{2[1 + S_{2s}(R_0)]}} \quad (26)$$

$$F_{(1s)3\sigma_g}(\mathbf{p}_N, \mathbf{R}_0) = \sqrt{N_e^{(3\sigma_g)}} C(\kappa_n) \frac{2^{5/2} \kappa_n^{5/2}}{\pi (p_N^2 + \kappa_n^2)^2} \frac{\cos[(\mathbf{p}_N \cdot \mathbf{R}_0)/2]}{\sqrt{2[1 + S_{1s}(R_0)]}} \quad (27)$$

$$F_{(2p)1\pi_g}(\mathbf{p}_N, \mathbf{R}_0) = -i\sqrt{N_e^{(1\pi_g)}} C(\kappa_n) \frac{2^5 \kappa_n^{7/2} p_N \sin(\theta_{\mathbf{p}})}{\pi \sqrt{2} (p_N^2 + \kappa_n^2)^3} \frac{\sin[(\mathbf{p}_N \cdot \mathbf{R}_0)/2]}{\sqrt{2[1 + S_{1s}(R_0)]}} \quad (28)$$

with the polar angle $\theta_{\mathbf{p}}$ of photoelectron emission relative to internuclear molecular axis ($\cos(\theta_{\mathbf{p}}) = (\mathbf{p} \cdot \mathbf{R}_0)/pR_0$) and $N_e^{(3\sigma_g)} = 2$ and $N_e^{(1\pi_g)} = 4$. Here $\kappa_n = Z_j^{(n)}/a_j$, whereas $Z_j^{(n)}$ is the effective charge corresponding to "effective" long-range Coulomb model binding potential of respective residual molecular ion, while $a_j = ja_0$ is j -th Bohr orbital radius of respective atomic orbital contributing to n -th initial molecular discrete state of molecular binding energy $\varepsilon_0^{(n)} = -\kappa_n^2/2 = -I_p^{(n)} = -(Z_j^{(n)}/a_j)^2/2$ under consideration (viz., $\varepsilon_0^{(3\sigma_g)}(N_2) \approx -15.58$ eV, $\varepsilon_0^{(1\pi_g)}(O_2) \approx -12.13$ eV). The analytical expressions for respective atomic orbital overlap integrals (19) are presented in [31], moreover, due to the VG version of SFA applied, the correction factor $C(\kappa_n) = (2\kappa_n I_p^{(n)}/E)^{\kappa_n^{-1}}$ is also introduced to matrix elements (25)-(28) to incorporate the long-range electron-molecular ion Coulomb interaction in the final continuum *Volkov states* into account [19].

Let's note first that the angular dependence of the $(2p)3\sigma_g$ molecular wavefunction in momentum space (25) clearly indicates that a separate contribution from $2p_z$ states alone is highly resistant to ionization along the direction perpendicular to the internuclear molecular axis ($\cos(\theta_{\mathbf{p}}) \approx 0$). The respective angular dependence on the angle $\theta_{\mathbf{p}}$ of photoelectron emission relative to the internuclear axis is well seen in Fig.1a to be a considerably prolate along the internuclear axis. Thus, the photoelectron emission from $(2p)3\sigma_g$ MO is profoundly dominated along the internuclear molecular axis ($\cos(\theta_{\mathbf{p}}) \approx 1$). similar to observed earlier in [31] for incorrect (the "+") combination of two $2p_z$ states. This, particularly, illustrates that the spatial (gerade or ungerade) symmetry of the $(2p)3\sigma_g$ MO doesn't essentially affect the angular dependence (viz., *nodal plane* along the molecular axis) of respective Fourier transform. Owing to the presence of $\cos(\theta_{\mathbf{p}})$ factor (see Eq.(25)), both the "-" (currently used) and the "+" (earlier used in [31]) combination of $2p_z$ atomic states suggest a predominant photoelectron emission along the internuclear axis (see also Fig.1a presented in [31], for comparison). The sign of the combination mostly alters the absolute value of local maxima in respective Fourier transform due to different (*sine* or *cosine*) trigonometric factor arising due to intramolecular interference of contributions of ionization from two atomic centers [19] separated by the internuclear distance R_0 . Since the generalized Bessel functions in Eqs.(10)-(11) are commonly maximized when photoelectron momentum \mathbf{p} is parallel to the laser polarization \mathbf{e} , the

ionization from $(2p)3\sigma_g$ HOMO composed as a single combination of $2p_z$ states alone is thus expected to be predominant when N_2 molecular axis is aligned along the laser field polarization ($\mathbf{R}_0 \parallel \mathbf{e}$). The latter conclusion (also previously made in [31] for $(2p)3\sigma_g$ HOMO of ungerade symmetry) seems to be natural and consistent with relevant experiment [32] and earlier alternative VG-SFA calculation [19] (see Fig.7b presented therein) using pure numerical self-consistent Hartree-Fock (HF) procedure of $3\sigma_g$ HOMO composition taking the contribution from atomic s -states into account. However, this statement is in a contradiction to respective VG-SFA results of calculation [33] applying the same VG-SFA approach and numerical HF-based procedure of $3\sigma_g$ composition as proposed earlier in Ref.[19]. Contrary to [19], the strong-field ionization of N_2 was found in [33] to be predominant for perpendicular orientation of internuclear axis relative to the laser field polarization.

To clarify the reason of the contradiction, Figures 1b-1d demonstrate the angular dependence of molecular wavefunction in momentum space calculated for possible different $3\sigma_g$ compositions (5), either with or without taking a comparable contribution from atomic s -states into account. The relative (weight) coefficients A_j at $1s$, $2s$ and $2p_z$ states under consideration proved to have comparable values for $3\sigma_g$ composition presented in Fig.1, although not necessarily of the same signs. For example, $A_{1s} \simeq -A_{2p} \approx 1/\sqrt{2}$ for $(1s2p)3\sigma_g$, whereas $A_{1s} \simeq -A_{2s} \simeq -A_{2p} \approx 1/\sqrt{3}$ for $(1s2s2p)3\sigma_g$ composition, so that the weight coefficients at $1s$ and $2p_z$ states (as well as $1s$ and $2s$ states) are found to have always opposite signs. Moreover, only the combinations with A_{1s} and A_{2p} (as well as A_{1s} and A_{2s}) of opposite signs proved to provide no suppression in N_2 ionization revealed in experiment [26]. To summarize, the presented Fourier transforms corresponding to $(1s2p)3\sigma_g$ and/or $(1s2s2p)3\sigma_g$ valence shells clearly suggest a predominant photoelectron emission from $3\sigma_g$ HOMO along the internuclear axis, contrary to suggested in [33]. Our Fig.1 also demonstrates that such difference may only arise owing to relative contribution from s -states, which seems to be somehow *overestimated* (compared to p -states) within the particular $(12s7p)/[6s4p]$ basis chosen in [33] for numerical HF-based procedure of $3\sigma_g$ composition in coordinate space (see also [34] for details). In the meantime, a composition overestimating the relative contribution from s -states doesn't seem to be suitable to $3\sigma_g$ molecular state, which is known to have a more complex structure surely *dominated* by p -states in coordinate space [17]. This also becomes especially evident owing to Fig.12 in Ref.[35] displaying the correct orbital shape for the $3\sigma_g$ wavefunction in N_2 , which obviously contrasts with the resulting $3\sigma_g$ state of substantially different shape and detailed structure suggested in [33] (cf., for example, respective Fig.1c presented in the last reference therein).

For laser-irradiated atomic counterparts of diatomics under consideration - such as Ar (for N_2 and/or H_2) and Xe (for O_2) with $3p$ and $5p$ outermost atomic valence shells, respectively - the initial atomic ground state can be also approximately reproduced by corresponding one-electron hydrogen-like atomic orbital. The analytical expression for respective atomic Fourier transforms $F_{3p_z}^{(3p_x, 3p_y)}(\mathbf{p})$ of $3p_z$, $3p_x$ and $3p_y$ hydrogen-like AOs (e.g., in Ar) corresponding to different possible values of associated magnetic quantum number m (0 - for $3p_z$ and ± 1 - for $3p_x \pm i3p_y$) has the form:

$$F_{3p_z}^{(3p_x \pm i3p_y)}(\mathbf{p}_N) = \frac{iC(\kappa_n)2^4\sqrt{2}\kappa_n^{11/2}p_N}{\pi\sqrt{3}(p_N^2 + \kappa_n^2)^4} \begin{pmatrix} \pm \sin(\theta) \exp(\pm i\varphi) \\ \sqrt{2} \cos(\theta) \end{pmatrix} \quad (29)$$

Here the angles θ and φ are the polar and azimuthal angles of photoelectron emission with respect to the incident field polarization ($\cos(\theta) = (\mathbf{e} \cdot \mathbf{p})/p$), so that the angular

factor in the right-hand side of (29) corresponds to the case of either $3p_x \pm i3p_y$ (the upper part), or $3p_z$ (the lower part) AO. The "effective" charge $Z_{eff}^{(n)}$ of pure Coulomb model binding potential corresponds to the experimental value of atomic ionization potential $I_p = \kappa_n^2/2 = (Z_{eff}^{(n)}/a_3)^2/2$. ($I_p \approx 15.75$ eV - for Ar and $I_p \approx 12.13$ eV - for Xe).

The proposed strong-field model is also equally well suitable to describe molecular HHG process in arbitrary molecular valence shell including inner ones closest to the HOMO (although, of higher binding energy, different orbital symmetry and number of identical electrons). The contributions from different (outermost and inner) valence shells are to be added *coherently* in molecular HHG, so that total amplitude of emission of N -th harmonic is just the sum of respective partial amplitudes corresponding to contribution from each molecular valence shell under consideration. In particular, the overall N -th partial amplitude (4) of harmonic emission in diatomic N_2 can be represented as consisting of contributions from three highest molecular valence shells - $3\sigma_g$ ($I_p^{(3\sigma_g)} \approx 15.58$ eV), $1\pi_u$ ($I_p^{(1\pi_u)} \approx 16.96$ eV) and $2\sigma_u$ ($I_p^{(2\sigma_u)} \approx 18.73$ eV):

$$f_N^{(N_2)}(\Omega_{\mathbf{k}'}) = f_N^{(3\sigma_g)}(\Omega_{\mathbf{k}'}) + f_N^{(1\pi_u)}(\Omega_{\mathbf{k}'}) + f_N^{(2\sigma_u)}(\Omega_{\mathbf{k}'}) \quad (30)$$

whereas, for HHG in diatomic O_2 , accordingly, as contribution from three different highest molecular valence shells - $1\pi_g$ ($I_p^{(1\pi_g)} \approx 12.07$ eV), $1\pi_u$ ($I_p^{(1\pi_u)} \approx 16.26$ eV) and $3\sigma_g$ ($I_p^{(3\sigma_g)} \approx 18.18$ eV):

$$f_N^{(O_2)}(\Omega_{\mathbf{k}'}) = f_N^{(1\pi_g)}(\Omega_{\mathbf{k}'}) + f_N^{(1\pi_u)}(\Omega_{\mathbf{k}'}) + f_N^{(3\sigma_g)}(\Omega_{\mathbf{k}'}) \quad (31)$$

Under the conditions of equivalent atomic centers and the atomic or molecular specie occupies the same state before and after the passage of the laser pulse, only odd harmonics of the fundamental laser frequency of linear polarization are emitted [29]. The harmonic emission rates are to be currently calculated only for high-order harmonics of polarization $\mathbf{e}_{\mathbf{k}',\lambda'}$, for which the emission rate becomes maximal, that is parallel to polarization \mathbf{e} of incident laser field. The model-related background analytical expressions (3)-(12) and (25)-(28) do imply fully 3D consideration of the process (particularly, they are available for arbitrary orientation of internuclear molecular axis with respect to the laser polarization \mathbf{e}), nonetheless, the molecular axis is supposed further to be strongly aligned along the polarization of incident laser field (i.e. $(\mathbf{e} \cdot \mathbf{R}_0) \sim \cos(\Theta) = 0$) throughout our present consideration, unless stated otherwise. The associated *orientation effects* in molecular harmonic generation are thus beyond the scope of our present consideration, which is mostly focused on behavior of molecular harmonic spectra depending on equally important problem parameters, such as internuclear separation R_0 and properties of a specified laser-irradiated diatomic (such as orbital symmetry, composition and structure of molecular valence shells) as well as incident laser parameters (such as laser intensity, pulse duration and temporal profile).

4. CALCULATION, NUMERICAL RESULTS AND DISCUSSION.

When studying the strong-field phenomena, the major difficulty with molecules is to deal with both the electronic and the nuclear degrees of freedom (i.e., related to the molecular vibrational and rotational motion). Nonetheless, the including of the nuclei motion into a proper consideration is generally feasible within frame of the currently applied approach, but this additionally requires of preliminary knowing available reliable

data (previously calculated or measured in experiment) related to dependence of molecular binding energy on internuclear separation R_0 . To the best of our knowledge, the latter dependence is reliably known only for the simplest diatomics (H_2^+ or H_2), solely for which the R_0 -dependent behavior of molecular HHG can be numerically studied within the currently proposed model. For all other diatomics under consideration (N_2 and O_2), the nuclei motion will be further completely ignored and the *Born-Oppenheimer approximation* is supposed to be valid. For this reason we start our numerical study from H_2^+ molecular ion, which is sufficiently well explored in previous theoretical and experimental studies (see [36], for a review). Beginning from the first HHG calculations [37, 38], this molecular specie, owing to its structural simplicity, became the object of a large number of other theoretical and experimental investigations (e.g., [8, 10-12]), the results of which can be used for direct comparison.

Fig.2 displays our results for high-harmonic spectra of H_2^+ calculated as harmonic emission rates (13) compared to respective atomic counterparts of nearly identical binding energy under conditions considered earlier in [10]. Like in [10], the results presented in Fig.2a were calculated assuming R_0 -independent fixed molecular binding energy ε_0 (viz., $|\varepsilon_0| = 0.4$ a.u. for any internuclear separation R_0), which is supposed to be identical to that of model atomic "counterpart" bound to model zero-range potential (ZRP). Since the molecular binding energy is known to be R_0 -dependent, Fig.2b also presents the analogous high-harmonic spectra of H_2^+ calculated under the same laser pulse and R_0 -dependent molecular binding energy $\varepsilon_0(R_0)$ corresponding to initial $1\sigma_g$ ground state. Also, unlike Fig.2a, the high-harmonic spectrum of respective atomic "counterpart" was calculated assuming the hydrogen-like $1S$ discrete state of atomic binding energy $\varepsilon_0 \approx -15.86$ eV nearly identical to the molecular binding energy $\varepsilon_0 \approx -0.583$ a.u. of H_2^+ ($1\sigma_g$) corresponding to $R_0 = 12$ a.u. The molecular harmonic spectra presented in Fig.2 show the clear signs of the so-called "low-energy hump" similar to that revealed in [10] within a low-frequency domain, which is enormously enhanced for two-centered case as compared to the one-centered ("atomic") case also presented in Fig.2. The origin of this "hump" arising in molecular high-harmonic spectra was well explained earlier [10] in terms of the *rescattering* mechanism and, particularly, by the existence of two different pathways for the initially released electron to recombine: with the center it started from as well as with the other. Namely, the "hump" corresponds to the case when the initially released electron moves directly from one center to the other within a time interval that is short compared with the period of the field, moreover, this happens around the time where the field is near its maximum. Under these conditions the energy gain, which the released electron acquires from the driving laser field when moving along the shortest way from one atomic center to other, can be approximately evaluated just by $\varepsilon_{el} \sim ER_0$ that corresponds the position of the top harmonic $N_h \approx ER_0/\omega$ of the "hump". According to this quasiclassical interpretation, the position of its top harmonic should be noticeably shifted toward a higher frequency part for a larger internuclear separation R_0 . This particular behavior is fairly well reproduced in Fig.3 by other high-harmonic spectra of H_2^+ calculated for a different incident laser pulse and various larger values of R_0 , for which Fig.3 also shows the signs of "split" arising within the "low-energy hump".

We also note the position of high-frequency plateau cutoff calculated for relatively large internuclear separation and presented in Figures 2 and 3 noticeably deviates from what is prescribed by the well known rule " $I_p + 3.17U_p$ " for standard harmonic cutoff frequency. So, according to this rule, one would expect for the position N_C of the cutoff frequency to be nearly at the harmonic order $N_C \approx 43$ in Fig.2a or $N_C \approx 49$ in Fig.2b, that

is quite consistent with those figures suggest for atomic case. Meanwhile, the respective molecular harmonic spectra calculated for $R_0 = 12 \text{ a.u.}$ clearly demonstrate a noticeably different position for the cutoff frequency, viz., at harmonic order $N_C \approx 51$ in Fig.2a or $N_C \approx 55$ in Fig.2b. Moreover, there is also a pronounced and well-defined "cutoff split" visible within the plateau cutoff domain of molecular harmonic spectra presented in Figs.2, 3. This "cutoff split" is similar to the split revealed earlier [10] in the cutoff domain of H_2^+ high-harmonic spectra calculated for sufficiently large internuclear separation R_0 . The origin of the "cutoff split" can be also well explained in terms of the rescattering mechanism and, particularly, attributed to the interference of two other (longest, but topologically different) pathways for the released electron moving from the one atomic center to the other to recombine with (see, also [10], for details). The respective separation in energy the released electron gains from the driving laser field is about at the position of high-frequency plateau cutoff (viz., nearly around the mentioned above harmonic order $N = 47$ in Fig.2a and/or $N = 51$ in Fig.2b), so that the two maxima alongside completely mask the actual cutoff position as the distance R_0 increases.

As noted above, unlike the atomic case, the cutoff position N_C in calculated molecular harmonic spectra proved to be not fixed yet even for the fixed parameters of incident laser pulse, but also substantially dependent on internuclear separation. Such R_0 -dependent behavior of $N_C(R_0)$ is well illustrated by Fig.3, which represents H_2^+ harmonic spectra calculated for different fixed values of R_0 under the same laser pulse. In particular, Fig.3 demonstrates the deviation of the harmonic cutoff position from the well known rule " $I_p + 3.17U_p$ ", even if the corresponding decrease of molecular ionization potential I_p for larger R_0 is taken into complete account. So, in Fig.3a the position of high-frequency cutoff for relatively small $R_0 = 4 \text{ a.u.}$ is in a full accordance with the aforementioned rule for standard cutoff corresponding to the harmonic order $N_C \approx 73$. This value is accordingly and noticeably smaller compared to $N_C \approx 80$ prescribed for larger ionization potential $I_p = 30.0 \text{ eV}$ corresponding to the equilibrium internuclear separation $R_0 = 2 \text{ a.u.}$ Thus, the calculated position of harmonic cutoff initially moves toward a lower frequency domain of spectrum due to corresponding decrease of molecular ionization potential I_p as R_0 increases. However, under further expansion and corresponding decrease of molecular ionization potential, the cutoff frequency is, nevertheless, getting to move back toward a higher frequency domain, contrary to the "standard cutoff" rule. So, for example, in molecular harmonic spectra calculated for larger internuclear separation and presented in Fig.3a, one can identify the cutoff position located at harmonic order $N_C(R_0 = 15 \text{ a.u.}) \approx 79$ and $N_C(R_0 = 30 \text{ a.u.}) \approx 89$ respectively. These two values are noticeably larger than $N_C \approx 70$ prescribed by the mentioned "standard cutoff" rule based on correspondingly decreased molecular ionization potential in H_2^+ taken into account. The physical mechanism underlying this quite an opposite tendency of increasing the harmonic cutoff frequency for sufficiently large R_0 increased can be again well understood in terms of semiclassical "recollision" picture invoked above for interpretation of the "cutoff split". Namely, when R_0 increases, the released electron acquires an additional energy gain from the driving laser field when moving along the longer ways from one atomic center to other. Due to the mentioned additional energy gain followed by recombination the acquired electron energy is released as a photon of a considerably higher frequency that gives rise to increasing of the harmonic cutoff frequency. Beginning from sufficiently large internuclear separation (over about $R_0 = 10 \text{ a.u.}$), this mechanism becomes predominant, insomuch that the related additional energy gain can compensate or even overcome the competing decrease of standard cutoff frequency due to diminished molecular ionization

potential I_p for larger R_0 . Such a complicated R_0 -dependent behavior of harmonic cutoff position revealed in molecular high-harmonic spectra under discussion seems to be very promising for various applications. To the best of our knowledge, the dissociating diatomics with large internuclear separations were predicted first in [39] to be capable to produce high harmonics of frequency far beyond the "standard" (atomic) cutoff, however, this idea has not been confirmed yet by experiments. Particularly, when the nuclei are separated by a distance equal to odd multiples of $\pi\alpha_0$ (where $\alpha_0 = (E/\omega^2)$ is the classical amplitude of electron's excursion in laser field), the cutoff limit was shown to extend beyond $I_p + 3.17U_p$ up to $I_p + 8U_p$ since the limit of $8U_p$ is the maximum kinetic energy reachable by the electron during its classical excursion from one atomic center to other (see also [10]). The results presented in Fig.3 generally confirm such a prediction and indicate unambiguously that, quite a noticeable *extension* of high-frequency plateau cutoff is to be present in molecular harmonic spectra for very large internuclear separation. Although, due to relatively small values of R_0 used under calculations compared to $\pi\alpha_0 \approx 110 \text{ a.u.}$, the calculated extension of high-frequency plateau is not very impressive.

On the other hand, the values of R_0 considered in Figures 2, 3 proved to be sufficiently large to confirm the result of previous research [10, 38] showing that molecular harmonic spectra do not obey the " $I_p + 3.17U_p$ " rule yet for the position of high-frequency cutoff. Moreover, unlike atomic high-harmonic spectra, the molecular harmonic cutoff is split due to intramolecular interference and this "cutoff split" well seen to be a noticeably broader and more pronounced for larger R_0 . Also, like in [10], the currently calculated H_2^+ harmonic spectra in Fig.3 clearly demonstrate a significant enhancement (up to several orders of magnitude) in harmonic emission rate as internuclear separation R_0 increases. This is not surprising for diatomics since the respective molecular binding energy $|\varepsilon_0(R_0)|$ is to be smaller for larger R_0 . The similar enhancement of harmonic emission due to decreased ionization potential was initially revealed in atomic high-harmonic spectra (see, e.g., Fig.5 and Fig.10 in [40] as well as references to relevant experiments cited therein). This also allows for quite a clear explanation, namely, the laser-irradiated species having a smaller ionization potential are generally more polarizable, so that their response to the incident laser field is expected to be a noticeably stronger than in harder ionized species. Our results calculated for H_2^+ and presented in Fig.3 also confirm that the similar underlying physical mechanism is responsible for the enhancement of harmonic emission rate in diatomics for larger internuclear separation as well as the transient enhancement of the high-harmonic conversion efficiency recently found as exceeding the atomic one in expanding molecules [12, 14]. It is also very interesting that Fig.3 still demonstrates noticeable differences in details of two high-harmonic spectra of H_2^+ corresponding to different $1\sigma_g$ and $1\sigma_u$ initial molecular states and calculated for large $R_0 = 30 \text{ a.u.}$, at which generic structural features (e.g., such as orbital symmetry) of particular laser-irradiated diatomic are expected to have a very minor importance.

Another remarkable feature well recognized in molecular harmonic spectra presented in Fig.3a is a sufficiently pronounced local minimum clearly visible within the high-frequency plateau region and located respectively at $N = 55$ for $R_0 = 4 \text{ a.u.}$, $N = 53$ for $R_0 = 15 \text{ a.u.}$ and $N = 49$ for $R_0 = 30 \text{ a.u.}$ The minima seem to be similar to those revealed earlier in numerically calculated molecular high-harmonic spectra [11] and predicted to arise in harmonic spectra of diatomics with HOMO of bonding symmetry due to *destructive* intramolecular interference of photoelectron emission from separated atomic centers to intermediate continuum states. Like in [11], the interference-related minimum in Fig.3a shows a regular dependence of its position on internuclear separation and, particularly,

moves toward a lower frequency domain with increase of R_0 . Such R_0 -dependent behavior is generally in accordance with the semiclassical (although, quite an *ad hoc*) interpretation given in [11] and related rule $N_{\min}^{(HHG)} = I_p/\omega + \pi^2/(2\omega R_0^2) \sim \pi^2/(2\omega R_0^2)$ suggested for location of the minimum. However, the harmonic spectra calculated under the conditions of [11] and presented in Fig.3a doesn't seem to confirm the above prediction for location of the minimum, but rather suggest a different (although, quite a raw) approximate rule $N_{\min}^{(HHG)} = (I_p + U_p)/\omega + \pi^2/(2\omega R_0^2)$. The presently suggested empirical rule seems to be similar to revealed earlier for the interference-related minimum arising in calculated molecular photoelectron spectra [10, 31] due to direct ATI in diatomics with HOMO of bonding symmetry. Therefore, the interference-related phenomena arising in molecular harmonic spectra should also allow for transparent interpretation similar to that given for molecular ATI [31]. In our opinion, this also remarkably demonstrates a close and intimate interrelation of molecular ATI and HHG processes.

Since the harmonic generation process is strongly related to ionization, one should also expect the enhanced harmonic emission rates in laser-irradiated species for which the ionization rate is also enhanced for some reason. On the other hand, for laser pulses of sufficiently high peak intensity I and long pulse duration τ , the enhanced ionization leads to a faster saturation of ionization and exhaustion of initial state of laser-irradiated system, which, after reaching the saturation of ionization, is unable to efficiently produce high-order harmonics anymore. This gives rise to quite a natural restriction imposed on standard cutoff frequency $I_p + 3.17U_p$ (with ponderomotive energy $U_p \sim I$), which thus cannot be extended yet under further increase of incident laser intensity I over the saturation intensity I_{sat} . Hence, the laser-irradiated species, such as H_2 and O_2 , showing a suppression in ionization rate (compared to counterpart systems of nearly identical ionization potential I_p) are expected to produce harmonics of considerably higher frequency corresponding to a longer high-frequency plateau with an extended cutoff due to a noticeably higher laser intensity I_{sat} that saturates ionization. The extension in high-harmonic spectra of O_2 relative to atomic Xe under respective laser saturation intensity was recently observed in experiment [13] and also partly reproduced in related MO-ADK calculations [13] based on the Lewenstein atomic HHG model [22].

In order to assess a possible extension of high-frequency plateau in molecular harmonic spectra of more complex diatomics, such as N_2 and O_2 , compared to respective atomic counterparts, one has to evaluate first the respective saturation laser intensity for each of laser-irradiated species under consideration. Fig.4 displays our results for total probability of ionization of O_2 , Xe , N_2 and Ar calculated under conditions of experiment [13] according to formula (16) extended to the diatomic case based on earlier developed SFA-LCAO model [31] as described in Sec.3 above. The respective saturation laser intensity I_{sat} is well identified in Fig.4 and defined as the intensity at which about 99% of laser-irradiated species being ionized by the end of the laser pulse duration. The results have been summarized in the Table I, which, for the convenience of direct comparison, also represents the respective results of [13] calculated according to MO-ADK theory [23].

Table I

Specie	N_2	Ar	O_2	Xe
HOMO AO	$(1s2s2p)3\sigma_g$	$3p^6$	$(2p)1\pi_g$	$5p^6$
R_0 (Å)	1.1		1.21	
I_p (eV)	15.58	15.75	12.07	12.13
I_{sat} (W/cm^2) present calculation	$3.75 \cdot 10^{14}$	$4.4 \cdot 10^{14}$	$2.5 \cdot 10^{14}$	$1.7 \cdot 10^{14}$
I_{sat} (W/cm^2) MO – ADK calculation[13]	$3.71 \cdot 10^{14}$	$4.4 \cdot 10^{14}$	$3.01 \cdot 10^{14}$	$1.75 \cdot 10^{14}$

The table demonstrates a fairly good consistence of our currently calculated results with the prediction of MO-ADK theory, except the saturation intensity calculated for O_2 . The deviation is explained by a different value of molecular ionization potential, viz. $I_p(O_2) = 12.56$ eV used in [13] (see, e.g., Table I presented therein), which is a slightly higher compared to the currently used experimental value $I_p(O_2) = 12.07$ eV [26]. This inevitably leads to an overestimated high suppression in ionization of O_2 relative to Xe , thereby giving rise to a noticeably overestimated value of the saturation laser intensity $3.01 \cdot 10^{14} W/cm^2$ as compared to $2.5 \cdot 10^{14} W/cm^2$ currently calculated.

The high-harmonic spectra of O_2 presented in Fig.5 demonstrate a noticeable extension compared to the spectrum of Xe calculated at respectively lower laser saturation intensity previously found (Fig.5b). At the same time, the extension of molecular high-frequency plateau and respective cutoff frequency currently calculated for O_2 (relative to Xe) noticeably deviates from the similar extension found in [13] for different saturation intensities calculated using the MO-ADK model. Particularly, the harmonic order N_C for cutoff position in presently calculated harmonic spectrum of O_2 is about 39 (versus calculated 43 and measured 53, both reported in [13]) provided the contribution from the $1\pi_g$ HOMO is only taken into account, like in [13]. However, the total harmonic spectrum of O_2 presented in Fig.5a and corresponding to the coherent contribution (31) from the $(2p)1\pi_g$ HOMO and two closest $(2p)1\pi_u$ and $(1s2s2p)3\sigma_g$ inner shells additionally taken into account demonstrate a noticeably longer high-frequency plateau of cutoff located at $N_C(O_2) = 45$ and thus extended relative to Xe , for which the cutoff is located at $N_C(Xe) = 29$. Note also that the additional extension clearly visible in Fig.5a is mostly due to the contribution from the inner $3\sigma_g$ valence shell, whose separate contribution within the cutoff domain is comparable with that from the $(2p)1\pi_g$ HOMO and always prevailing with respect to that from the $(2p)1\pi_u$, despite the inner $3\sigma_g$ has the higher ionization potential than $1\pi_g$ or $1\pi_u$. This noted feature seems to be quite a natural for strongly aligned diatomics under consideration and can be explained by an enhanced ionization (initial release of electron to intermediate continuum states) from the $3\sigma_g$ MO, which is a considerably prolate along the internuclear axis. Unlike σ orbitals, π molecular orbitals (such as $1\pi_g$ HOMO and inner $1\pi_u$ in O_2) are predominantly oriented along the direction perpendicular to the internuclear axis, so that the photoelectron emission (initial release of electron to intermediate continuum states) from π molecular orbitals in aligned diatomics is a considerably suppressed along the internuclear axis that leads to a relatively smaller harmonic emission rate (see also the relevant discussion in [31]).

The high-harmonic spectra of N_2 and its atomic counterpart Ar calculated for respective saturation intensities currently found and shown in Table I, are presented in Fig.6.

In particular, Fig.6b demonstrates some minor extension of cutoff in harmonic spectrum of Ar relative to N_2 due to a slightly enhanced ionization rate of N_2 observed in experiments [25, 26] and related lower laser saturation intensity compared to Ar . The cutoff position in currently calculated harmonic spectrum of N_2 corresponding to the separate contribution from the $(1s2s2p) 3\sigma_g$ HOMO (only taken into account in [13]) is located at harmonic order about 55 that is well consistent with that calculated in [13]. Meanwhile, the total harmonic spectrum of N_2 presented in Fig.6a and calculated taking the coherent contribution (30) from two closest inner $(2p) 1\pi_u$ and $(2s) 2\sigma_u$ valence shells into account demonstrates a bit longer plateau of cutoff position at harmonic order $N_C(N_2) = 61$ that is in a reasonably good accordance with experimental value measured in [13]. This noted extension of high-frequency plateau cutoff is also clearly visible to arise mostly due to $2\sigma_u$ valence shell, whose separate contribution within the cutoff region is comparable with that from the $3\sigma_g$ HOMO and always prevailing over that from $1\pi_u$, even though the ionization potential of $2\sigma_u$ is higher. Thus, the additional extension due to the contribution from inner valence shells is quite similar to that we observed earlier in the total high-harmonic spectrum of O_2 presented in Fig.5a. This probably might also explain the difference between the positions found for harmonic cutoff in high-harmonic spectra of N_2 calculated and observed in [13].

All the results presented in Fig.5 and Fig.6 have been summarized in Table II below, for the convenience of direct comparison with experiment [13].

Table II

Specie (AO, MO)	I_p (eV)	N_C presently calculated	N_C MO – ADK based calculation [13]	N_C measured in experiment [13]
$N_2 [(1s2s2p) 3\sigma_g]$	15.58	55	55	
$N_2 [(2p) 1\pi_u]$	16.96	57		
$N_2 [(2s) 2\sigma_u]$	18.73	57		
$N_2 (3\sigma_g + 1\pi_u + 2\sigma_u)$		61		57
$Ar (3p^6)$	15.75	67	65	63
$O_2 [(2p) 1\pi_g]$	12.07	39	45	
$O_2 [(2p) 1\pi_u]$	16.26	43		
$O_2 [(1s2s2p) 3\sigma_g]$	18.18	43		
$O_2 (1\pi_g + 1\pi_u + 3\sigma_g)$		45		53
$Xe (5p^6)$	12.13	29	29	29

As a final remark to the results presented in Table II, we have to comment the respective HHG results for N_2 and Ar reported in [13] and based on MO-ADK calculation of laser saturation intensity (see Table I in Ref.[13]). Namely, the latter results seem to be at least confusing and contradicting to the MO-ADK results presented *ibidem* in Fig.4, which unambiguously shows a considerable suppression for N_2^+ ion signal compared to Ar^+ for the shorter laser pulse of duration $\tau = 30$ fs. Under these conditions close to experiment [13] corresponding to $\tau = 25$ fs, the MO-ADK model suggests the calculated ratio N_2^+/Ar^+ for ion signals from N_2^+ relative to Ar^+ to be nearly around 0.5 (see also Fig.8 in [23]) that is consistent with relevant experiment [25], at least within the strong-field domain where the tunneling ionization theory is only valid. This, however, implies that the MO-ADK based calculation would result in an accordingly higher saturation intensity rather for N_2

than for *Ar*, similarly to the suppressed ionization in *O*₂ relative to *Xe*. Contrary to such a natural conclusion the calculated laser saturation intensity for *N*₂ was identified in [13] to be a noticeably lower (viz., $3.71 \cdot 10^{14} \text{ W/cm}^2$ versus $4.4 \cdot 10^{14} \text{ W/cm}^2$ reported for *Ar*) that seems to be self-contradicting and thus makes a fairly good agreement of the calculated and measured harmonic cutoff frequency of respective high-harmonic spectra observed in [13] quite a questionable and controversial.

5. CONCLUSION.

The strong-field process of high-order harmonic generation was considered and studied numerically in a number of laser-irradiated homonuclear diatomics (namely, *H*₂⁺, *N*₂ and *O*₂) compared to their atomic counterparts of nearly identical ionization potential. The proposed strong-field molecular HHG model is essentially based on quantum-mechanical SFA-based approach developed earlier and currently extended to molecular case using the standard LCAO-MO method applied for adequate reproducing the wavefunction of initial molecular discrete state. The latter wavefunction is approximately considered as a *single-electron* and *two-centered* molecular orbital (MO) consisting of coherent superposition of few predominantly contributing scaled hydrogen-like atomic orbitals (AO) centered on each of the atomic cores and thus separated by internuclear distance *R*₀. The form of contributing AOs is generally different for various molecular valence shells (such as σ_g , π_u and π_g) of different orbital and bonding symmetry. Wherever appropriate, the comparable contributions from other (inner) molecular valence shells of a larger binding energy and different orbital symmetry are also incorporated. This, particularly, allows for fully 3D consideration of molecular HHG process as well as deriving the final expressions for amplitude and rate of harmonic emission rate in closed analytical form available for further numerical calculations.

The calculated molecular high-harmonic spectra were found to exhibit a general shape similar to atomic ones, with extended high-frequency plateau ending by a well defined harmonic cutoff. Although, the detailed structure, such as the extent of high-frequency plateau and respective harmonic emission rates demonstrate a number of noticeable and remarkable differences from respective atomic harmonic spectra. These distinct differences, such as the "*low-frequency hump*" and "*cutoff split*" arising due to *two-centered* nature of molecular bound state, are ascertained to be strongly dependent on the internuclear separation *R*₀. For sufficiently large *R*₀ the molecular harmonic spectra demonstrate a plateau of a noticeably longer extent and significant enhancement in harmonic emission rates compared to spectra corresponding to equilibrium internuclear separation and calculated under the same laser pulses. In addition, our SFA calculations seem to confirm the existence of a broad and pronounced minimum predicted to arise in harmonic spectra of diatomics with HOMO of bonding symmetry due to *destructive* intramolecular interference of contribution from photoelectrons of large momenta emitted from separate atomic centers [11] to intermediate continuum states. Namely, our results presented in Fig.3a seem to reproduce *R*₀-dependent behavior of the interference-related minimum found in 1D and/or 2D TDSE calculations [11], although also suggest a bit different (compared to [11]) approximate rule for location of this minimum in molecular harmonic spectra.

Finally, the average harmonic emission rate proved to be very sensitive to orbital symmetry of molecular orbital and its predominant orientation with respect to the internuclear molecular axis, insomuch that for some group of harmonics the contribution from inner molecular shell of higher binding energy (but, different orbital symmetry) can

be comparable (or even predominant within the plateau cutoff region) relative to that from the HOMO. Also, due to a high suppression revealed in ionization rate for O_2 relative to Xe atom, the harmonic spectrum calculated for O_2 was found to demonstrate a high-frequency plateau of a considerably longer extent (and accordingly higher harmonic cutoff frequency) than in spectrum of Xe atom, for which the saturation laser intensity was calculated to be a noticeably smaller. To conclude, the numerically studied behavior of harmonic spectra calculated for O_2 , N_2 and H_2^+ depending on the problem parameters proved to be in a reasonable or fairly good accordance with relevant data calculated by earlier authors and observed in molecular HHG experiments.

6. ACKNOWLEDGMENTS.

This work was supported by the Chemical Sciences, Geosciences and Biosciences Division of the Office of Basic Energy Sciences, Office of Science, U.S. Department of Energy and also, separately, by the Center of Sciences and Technology of Uzbekistan (Project No. Φ -2.1.44). The support from DAAD (Deutscher Akademischer Austauschdienst) and B-Division of Max-Born-Institute of Nonlinear Optics and Short-Pulse Laser Spectroscopy (Berlin, Germany) is also gratefully acknowledged.

The research described in this presentation was made also possible in part by financial support from the U.S. Civilian Research and Development Foundation (CRDF) for the Independent States of the Former Soviet Union.

References

- [1] M. Hentschel, R. Kienberger, C. Spielmann, G.A. Reider, N. Milosevic, T. Brabec, P. Corkum, U. Heinzmann, M. Drescher and F. Krausz, *Nature* **414**, 509 (2001); H. C. Kapteyn, M. M. Murnane and I. P. Christov, *Phys. Today*, No.3 (March), 39 (2005).
- [2] C. Spielmann, N. H. Burnett, R. Sartania, R. Koppitsch, M. Schnurer, C. Kan, M. Lenzner, P. Wobrauschek, and F. Krausz, *Science* **278**, 661 (1997); C. Spielmann, C. Kan, N. H. Burnett, T. Brabec, M. Geissler, A. Scrinzi, M. Schnurer, and F. Krausz, *IEEE J. Sel. Top. Quant. Electr.* **4**, 249 (1998).
- [3] J. Itatani, J. Levesque, D. Zeidler, H. Niikura, H. Pepin, J. C. Kieffer, P. B. Corkum, and D. M. Villeneuve, *Nature* **432**, 867 (2004).
- [4] M. Protopapas, C. H. Keitel and P. L. Knight, *Rep. Prog. Phys.* **60**, 389 (1997).
- [5] P. Salières, A. LHuillier, P. Antoine, and M. Lewenstein, *Adv. At. Mol. Opt. Phys.* **41**, 83 (1999).
- [6] D. B. Milosevic and F. Ehlotzky, *Adv. At. Mol. Opt. Phys.* **49**, 377 (2003).
- [7] C. Lyngå, A. L’Huillier, and C.-G. Wahlström, *J. Phys. B* **29**, 3293 (1996).
- [8] D. G. Lappas and J. P. Marangos, *J. Phys. B* **33**, 4679 (2000).
- [9] R. Velotta, N. Hay, M. B. Mason, M. Castillejo and J. P. Marangos, *Phys. Rev. Lett.* **87**, 183901 (2001); N. Hay, R. Velotta, M. Lein, R. de Nalda, E. Heesel, M. Castillejo and J. P. Marangos, *Phys. Rev. A* **65**, 053805 (2002).

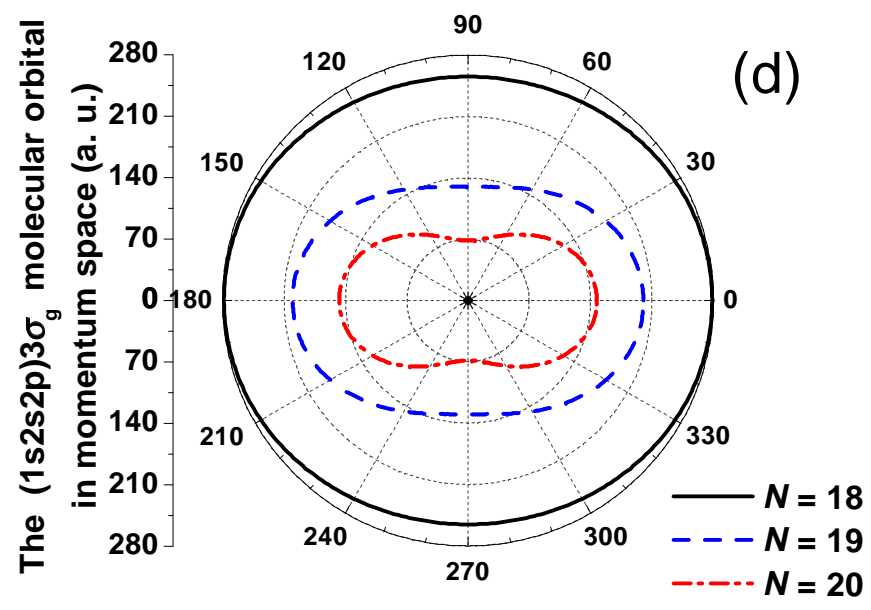
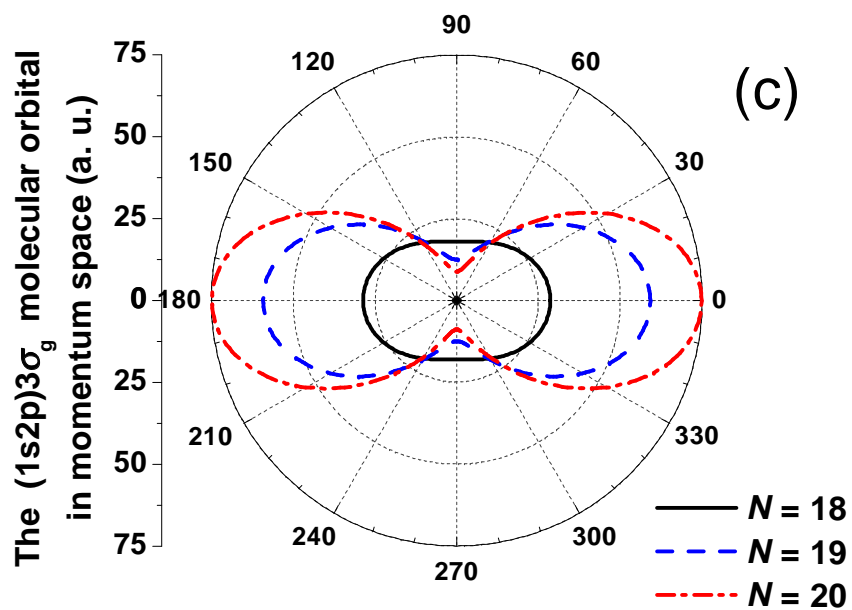
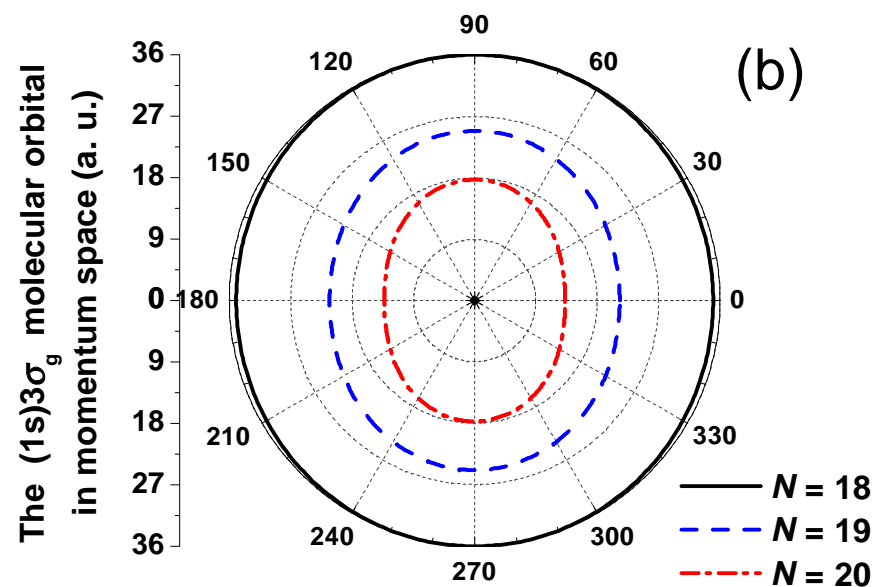
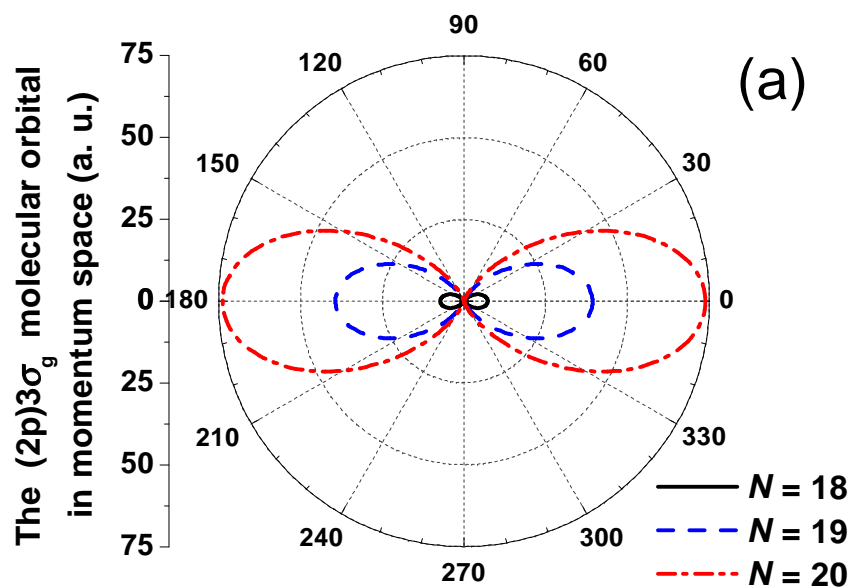
- [10] R. Kopold, W. Becker and M. Kleber, Phys. Rev. A **58**, 4022 (1998).
- [11] M. Lein, N. Hay, R. Velotta, J. P. Marangos and P. L. Knight, Phys. Rev. A **66**, 023805 (2002); Phys. Rev. Lett. **88**, 183903 (2002); M. Lein, P. P. Corso, J. P. Marangos and P. L. Knight, Phys. Rev. A **67**, 023819 (2003).
- [12] T. Pfeifer, D. Walter, G. Gerber, M. Yu. Emelin, M. Yu. Ryabikin, M. D. Chernobrovtsseva and A. M. Sergeev, Phys. Rev. A **70**, 013805 (2004).
- [13] B. Shan, X. M. Tong, Z. Zhao, Z. Chang, and C. D. Lin, Phys. Rev. A **66**, 061401(R) (2002).
- [14] D. A. Telnov and Shih-I Chu, Phys. Rev. A **71**, 013408 (2005).
- [15] T. Kanai, S. Minemoto, H. Sakai, Nature **435**, 470 (2005)
- [16] J. P. Marangos, Nature **435**, 435 (2005).
- [17] B. Zimmermann, M. Lein and J. M. Rost, Phys. Rev. A **71** , 033401 (2005).
- [18] H. D. Cohen and U. Fano, Phys. Rev. **150**, 30 (1966).
- [19] J. Muth-Böhm, A. Becker, and F. H. M. Faisal, Phys. Rev. Lett. **85**, 2280 2000 ; A. Jaron-Becker, A. Becker, and F. H. M. Faisal, Phys. Rev. A **69**, 023410 (2004).
- [20] H. R. Reiss, Prog. Quant. Electr. **16**, 1 (1992); H. R. Reiss, Phys. Rev. A **42**, 1476 (1990).
- [21] L. V. Keldysh, Zh. Exp. Teor. Fiz. **47**, 1945 (1964) [Sov. Phys. -JETP **20**, 1307 (1965)]; F. Faisal, J. Phys. B **6** , L312 (1973). H. R. Reiss, Phys. Rev. A **22**, 1786 (1980).
- [22] M. Lewenstein, P. Balcou, M. Y. Ivanov, A. L'Huillier, and P. B. Corkum, Phys. Rev. A **49**, 2117 (1994).
- [23] X. M. Tong, Z. X. Zhao, and C. D. Lin, Phys. Rev. A **66**, 033402 (2002).
- [24] M. V. Ammosov, N. B. Delone and V. P. Krainov, Sov. Phys. -JETP **64**, 1191 (1986).
- [25] C. Guo, M. Li, J. P. Nibarger and G. N. Gibson, Phys. Rev. A **58**, R4271 (1998).
- [26] E. Wells, M. J. DeWitt and R. R. Jones, Phys. Rev. A **66**, 013409 (2002); M. J. DeWitt, E. Wells and R. R. Jones, Phys. Rev. Lett. **87**, 153001 (2001).
- [27] Shih-I Chu, Adv. At. Mol. Phys. **21**, 197 (1985); Adv. Chem. Phys. **73**, 739 (1989); Shih-I Chu and D. A. Telnov, Phys. Rep. **390**, 1 (2004).
- [28] X.Chu and Shih-I Chu, Phys. Rev. A **63**, 023411 (2001); X.Chu and Shih-I Chu, Phys. Rev. A **64**, 063404 (2001).
- [29] V. I. Usachenko and V. A. Pazdersky, J. Phys. B **35** , 761 (2002).
- [30] V. I. Usachenko, V. A. Pazdersky and J. K. McIver, Phys. Rev. A **69**, 013406 (2004).
- [31] V. I. Usachenko and Shih-I Chu, Phys. Rev. A **71**, 063410 (2005).
- [32] I. V. Litvinyuk, K. F. Lee, P. W. Dooley, D. M. Rayner, D. M. Villeneuve, and P. B. Corkum, Phys. Rev. Lett. **90**, 233003 (2003).

- [33] T. K. Kjeldsen and L. B. Madsen, *J. Phys. B* **37**, 2033 (2004); *Phys. Rev. A* **71**, 023411 (2005); e-print arXiv:physics/0508213.
- [34] V. I. Usachenko, e-print arXiv:physics/0604068.
- [35] A. Scrinzi, M. Yu. Ivanov, R. Kienberger and D. M. Villeneuve, *J. Phys. B* **39**, R1 (2006).
- [36] A. Giusti-Suzor, F. H. Mies, L. F. DiMauro, E. Charron, and B. Yang, *J. Phys. B* **28**, 309 (1995).
- [37] M. Yu. Ivanov and P. B. Corkum, *Phys. Rev. A* **48**, 580 (1993).
- [38] T. Zuo, S. Chelkowski and A. D. Bandrauk, *Phys. Rev. A* **48**, 3837 (1993).
- [39] R. Numico, P. Moreno, L. Plaja and L. Roso, *J. Phys. B* **31**, 4163 (1998); P. Moreno, L. Plaja and L. Roso, *Laser Phys.* **7**, 602 (1997).
- [40] A. L'Huillier, K. J. Shafer and K. C. Kulander, *J. Phys. B* **24**, 3315 (1991).

FIGURE CAPTIONS

1. Fig.1. (Color online). The squared module $|F_{3\sigma_g}(\mathbf{p}_N, \mathbf{R}_0)|^2$ of molecular wavefunction in momentum space (Fourier transform) for N_2 vs the angle $\theta_{\mathbf{p}}$ (relative to the internuclear molecular axis lined up in the horizontal direction) of photoelectron emission from the $3\sigma_g$ HOMO of different composition: (a) $(2p)3\sigma_g$ MO composed from $2p_z$ states alone, (b) $(1s)3\sigma_g$ MO composed from $1s$ states alone, (c) $(1s2p)3\sigma_g$ MO composed from $1s$ and $2p_z$ states, (d) $(1s2s2p)3\sigma_g$ MO composed from $1s$, $2s$ and $2p_z$ states. Those angular dependencies are presented for photoelectrons only emitted along the laser field polarization due to absorption of different number N of laser photons beginning from minimum one $N_0 = 18$ required for ionization of the $3\sigma_g$ HOMO by *Ti:sapphire* incident laser field of the wavelength $\lambda = 800 \text{ nm}$ ($\hbar\omega = 1.55 \text{ eV}$) and fixed intensity $I = 2 \cdot 10^{14} \text{ W/cm}^2$.
2. Fig.2. (Color online). The differential harmonic emission rates $w_N^{(HHG)}(\mathbf{k}')$ [Eq.(13)] in strongly aligned H_2^+ vs the harmonic order N calculated under conditions of Ref.[10] for incident laser field of the wavelength $\lambda \approx 1064 \text{ nm}$ ($\hbar\omega = 1.172 \text{ eV}$) and intensity $I = 1.19 \cdot 10^{14} \text{ W/cm}^2$ (so that $\eta \approx 10.58$). The presented molecular high-harmonic spectra (filled circles) are for the internuclear separation $R_0 = 12 \text{ a.u.}$ assuming (a) the fixed (independent on R_0) binding energy ε_0 ($|\varepsilon_0| = 0.4 \text{ a.u.}$) (b) R_0 -dependent molecular binding energy $\varepsilon_0(R_0)$ corresponding to $(1s)1\sigma_g$ valence shell. The respective spectra of model counterpart "atom" (open circles) of the same ionization potential I_p were calculated assuming (a) the model zero-range binding potential (ZRP), (b) pure Coulomb binding potential. The results of Fig.2a are to be compared with relevant ones calculated within a different HHG model [10] (see Fig.4 presented therein).
3. Fig.3. (Color online). The differential harmonic emission rates $w_N^{(HHG)}(\mathbf{k}')$ [Eq.(13)] vs the harmonic order N calculated for various internuclear separations R_0 in H_2^+ strongly aligned along the polarization of *Ti:sapphire* laser field of the wavelength $\lambda \approx 800 \text{ nm}$ ($\hbar\omega = 1.55 \text{ eV}$) and intensity $I = 5 \cdot 10^{14} \text{ W/cm}^2$. The calculated harmonic spectra are presented for two different bonding symmetry of initial molecular state: (a) bonding $1\sigma_g$ molecular state, (b) antibonding $1\sigma_u$ molecular state. The molecular binding energy ε_0 is supposed to be dependent on internuclear separation R_0 , so that the dependence $\varepsilon_0(R_0)$ is to be different for $1\sigma_u$ and $1\sigma_g$ molecular orbitals. Beginning from $R_0 = 10 \text{ a.u.}$ the dependence $\varepsilon_0(R_0)$ becomes almost the same for $1\sigma_u$ and $1\sigma_g$ valence shells and, to a fairly good accuracy, can be approximately reproduced by the equation $\varepsilon_0(R_0) \approx -0.5 - 1/R_0$. These results are to be compared with relevant ones presented in Ref.[11] (see, e.g., Fig.4 therein).
4. Fig.4. (Color online). The temporal dependence of total ionization probability $P_{ion}(\tau)$ [Eq.(17)] calculated under conditions of experiment [13] for (a) diatomic O_2 , (b) atomic Xe , (c) diatomic N_2 , (d) atomic Ar irradiated by *Ti:sapphire* laser field of the wavelength $\lambda \approx 800 \text{ nm}$ and Gaussian temporal profile (16) with the pulse duration $\tau \approx 25 \text{ fs}$ corresponding to about 9.43 optical cycles. The presented results correspond to various values of laser peak intensity I : (a) $2.0 \cdot 10^{14} \text{ W/cm}^2$ (dash-dotted line), $2.2 \cdot 10^{14} \text{ W/cm}^2$ (dashed line) and the saturation intensity $2.5 \cdot 10^{14} \text{ W/cm}^2$ (solid line), (b) $1.5 \cdot 10^{14} \text{ W/cm}^2$ (dash-dotted line), $1.6 \cdot 10^{14} \text{ W/cm}^2$ (dashed line) and the saturation intensity $1.7 \cdot 10^{14} \text{ W/cm}^2$ (solid line), (c) $3.4 \cdot 10^{14} \text{ W/cm}^2$ (dash-dotted line), $3.6 \cdot 10^{14} \text{ W/cm}^2$ (dashed line) and the saturation intensity $3.75 \cdot 10^{14} \text{ W/cm}^2$ (solid line), (d) $4.0 \cdot 10^{14} \text{ W/cm}^2$ (dash-dotted line), $4.2 \cdot 10^{14} \text{ W/cm}^2$ (dashed line) and the saturation intensity $4.4 \cdot 10^{14} \text{ W/cm}^2$ (solid line).

5. Fig.5. (Color online). The differential harmonic emission rates $w_N^{(HHG)}(\mathbf{k}')$ [Eq.(13)] in laser-irradiated O_2 and its atomic counterpart Xe vs the harmonic order N calculated under conditions of experiment [13] for the laser pulse of respective saturation peak intensity presently found and summarized in Table I. (a) The spectra of O_2 corresponding to partial contributions from the $1\pi_g$ HOMO (open circles), the inner $1\pi_u$ (filled triangles) and $3\sigma_g$ (filled squares) valence shells separately are presented vs overall O_2 spectrum corresponding to coherent contribution (32) from those three highest-lying molecular valence shells under consideration put together (stars), (b) The overall harmonic spectrum of O_2 presented vs the Xe spectrum (filled diamonds) calculated for respective (different from O_2) saturation laser intensity. The results of Fig.5b are to be compared with relevant ones presented in Fig.5 of Ref.[13].
6. Fig.6. (Color online). The differential harmonic emission rates $w_N^{(HHG)}(\mathbf{k}')$ [Eq.(13)] in strongly aligned N_2 and its atomic counterpart Ar vs the harmonic order N calculated under conditions of experiment [13] for the laser pulse of respective saturation peak intensity presently found and summarized in Table I. (a) The spectra of N_2 corresponding to partial contributions from the $3\sigma_g$ HOMO (open circles), the inner $1\pi_u$ (filled triangles) and $2\sigma_u$ (filled squares) valence shells separately and presented vs overall N_2 spectrum corresponding to coherent contribution (31) from those three highest-lying molecular valence shells under consideration put together (stars). (b) The overall harmonic spectrum of N_2 (stars) presented vs two harmonic spectra of Ar calculated for two different laser peak intensities - $4.4 \cdot 10^{14} W/cm^2$ (filled diamonds) and $3.75 \cdot 10^{14} W/cm^2$ (open squares) corresponding to the saturation intensities found for ionization of Ar and N_2 , respectively. The results of Fig.6b are to be compared with relevant ones presented in Fig.5 of Ref.[13].



θ_p , Angle of Photoelectron Emission (degrees)

θ_p , Angle of Photoelectron Emission (degrees)

Fig.1

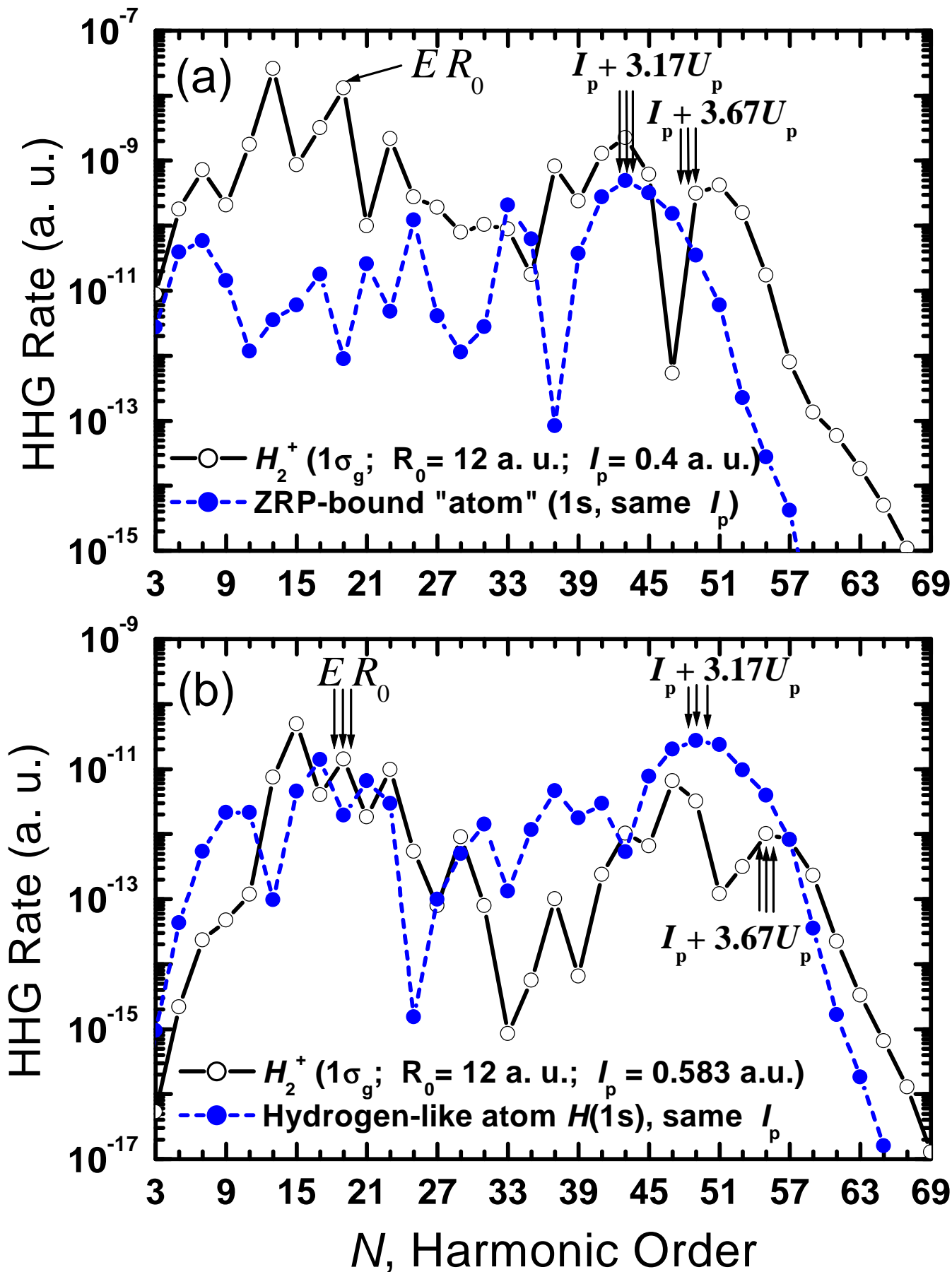


Fig. 2

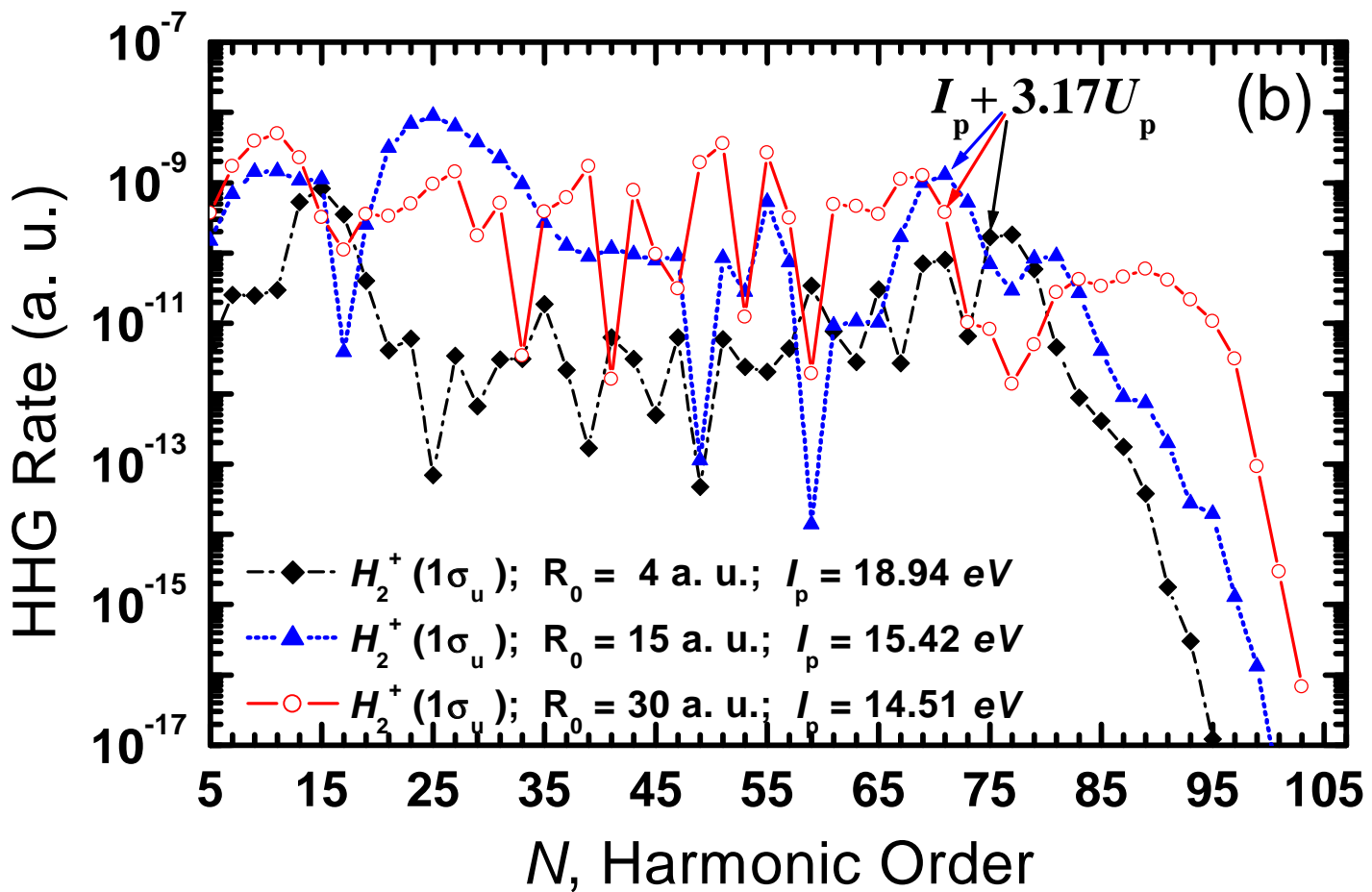
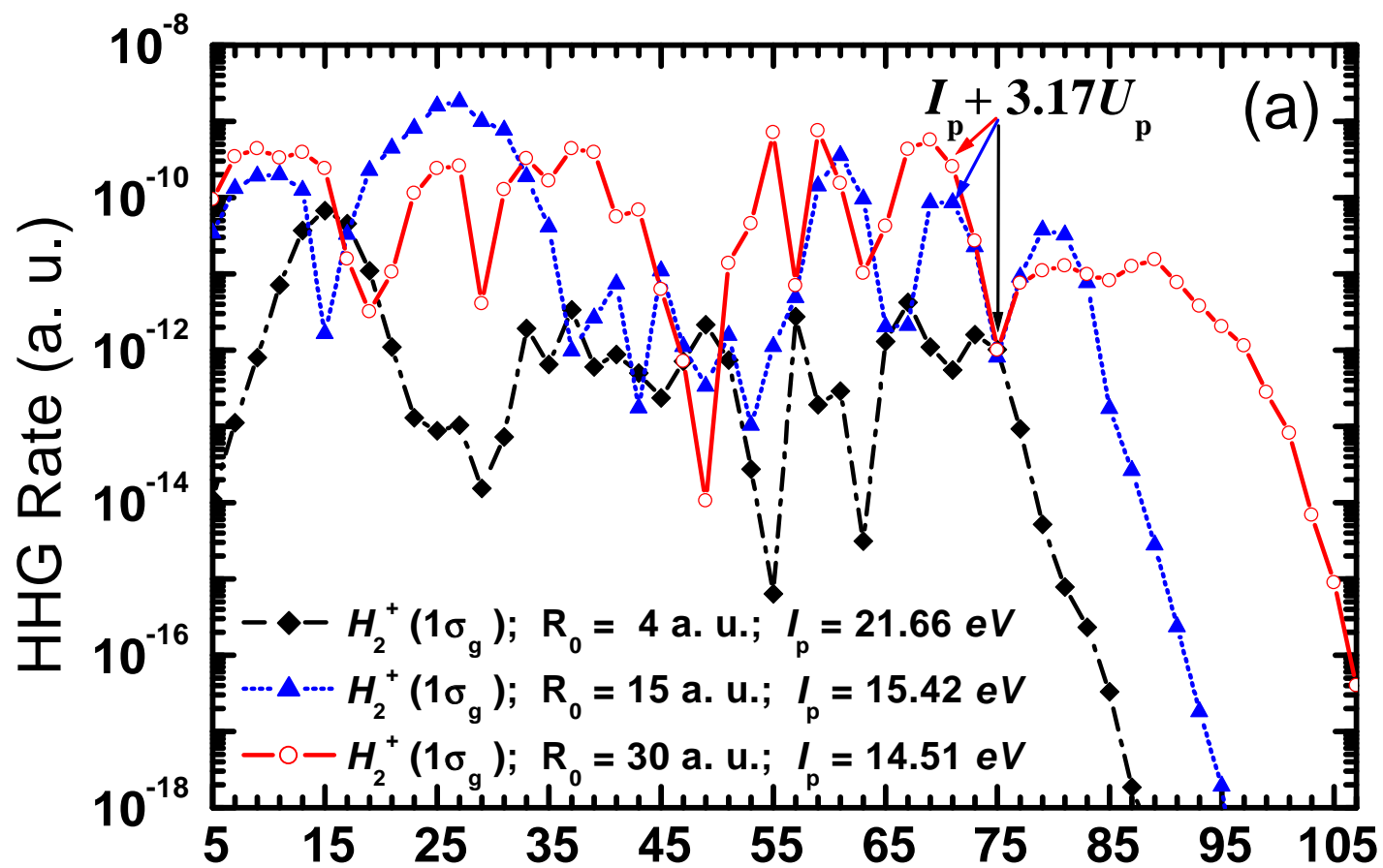


Fig. 3

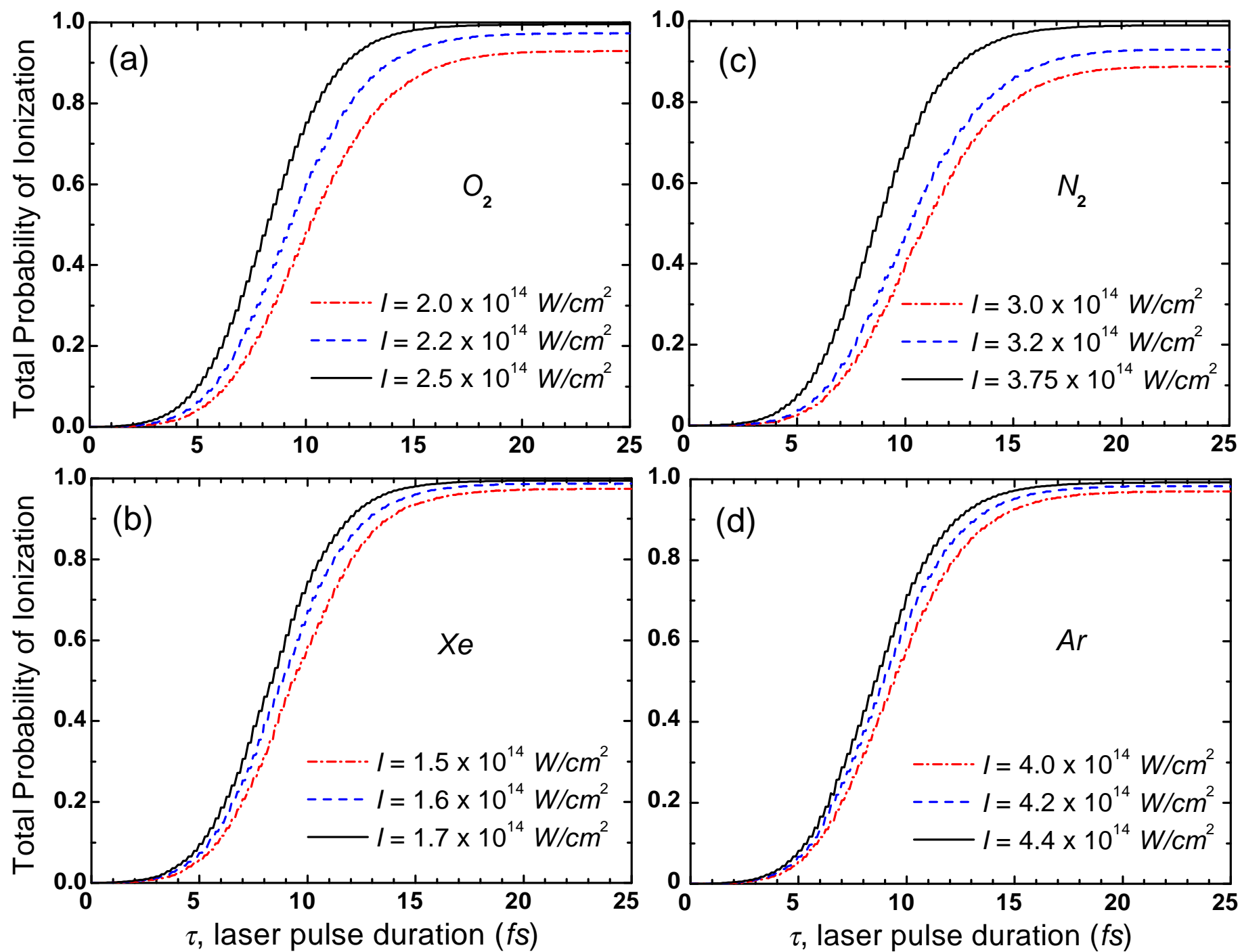


Fig. 4

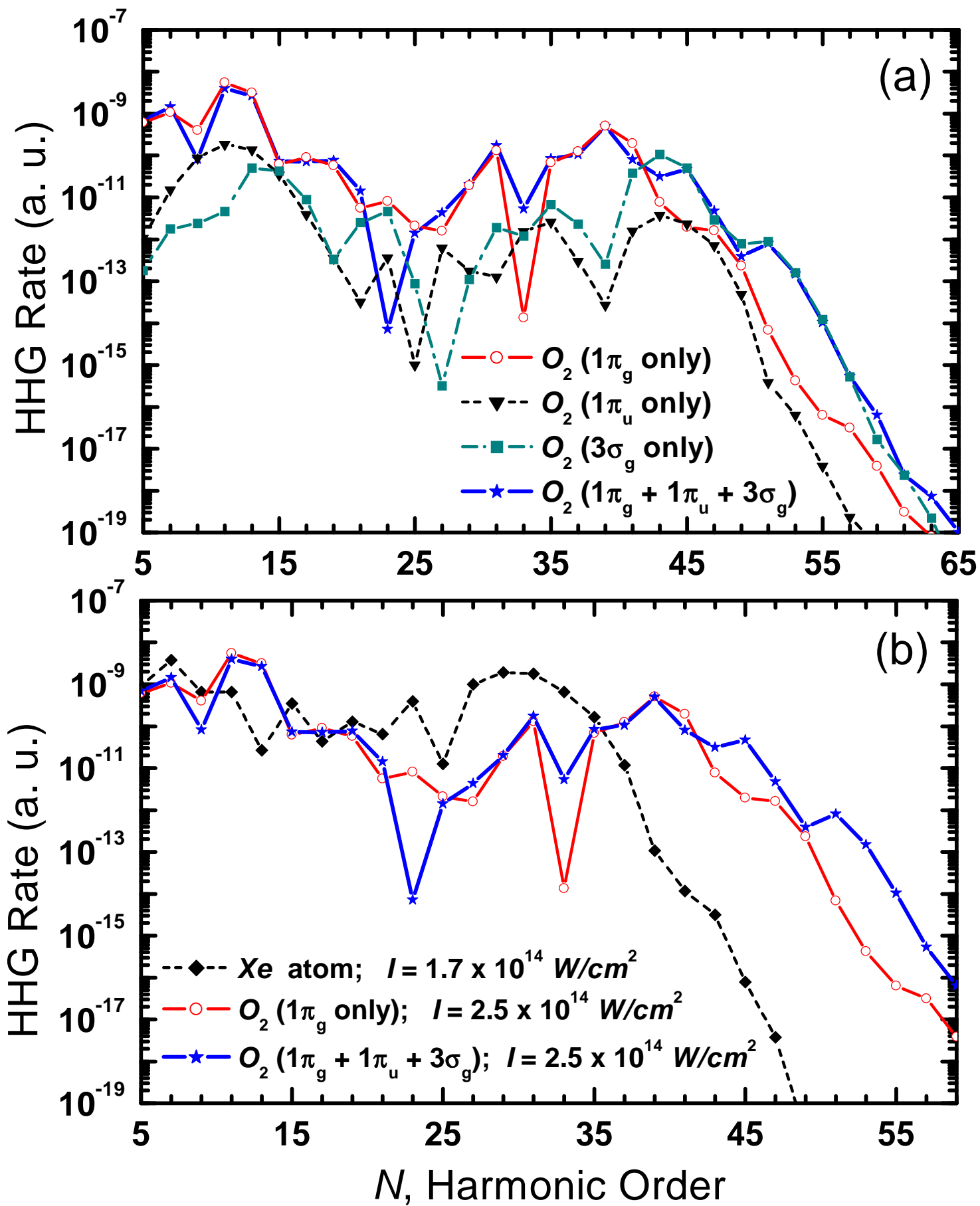


Fig. 5

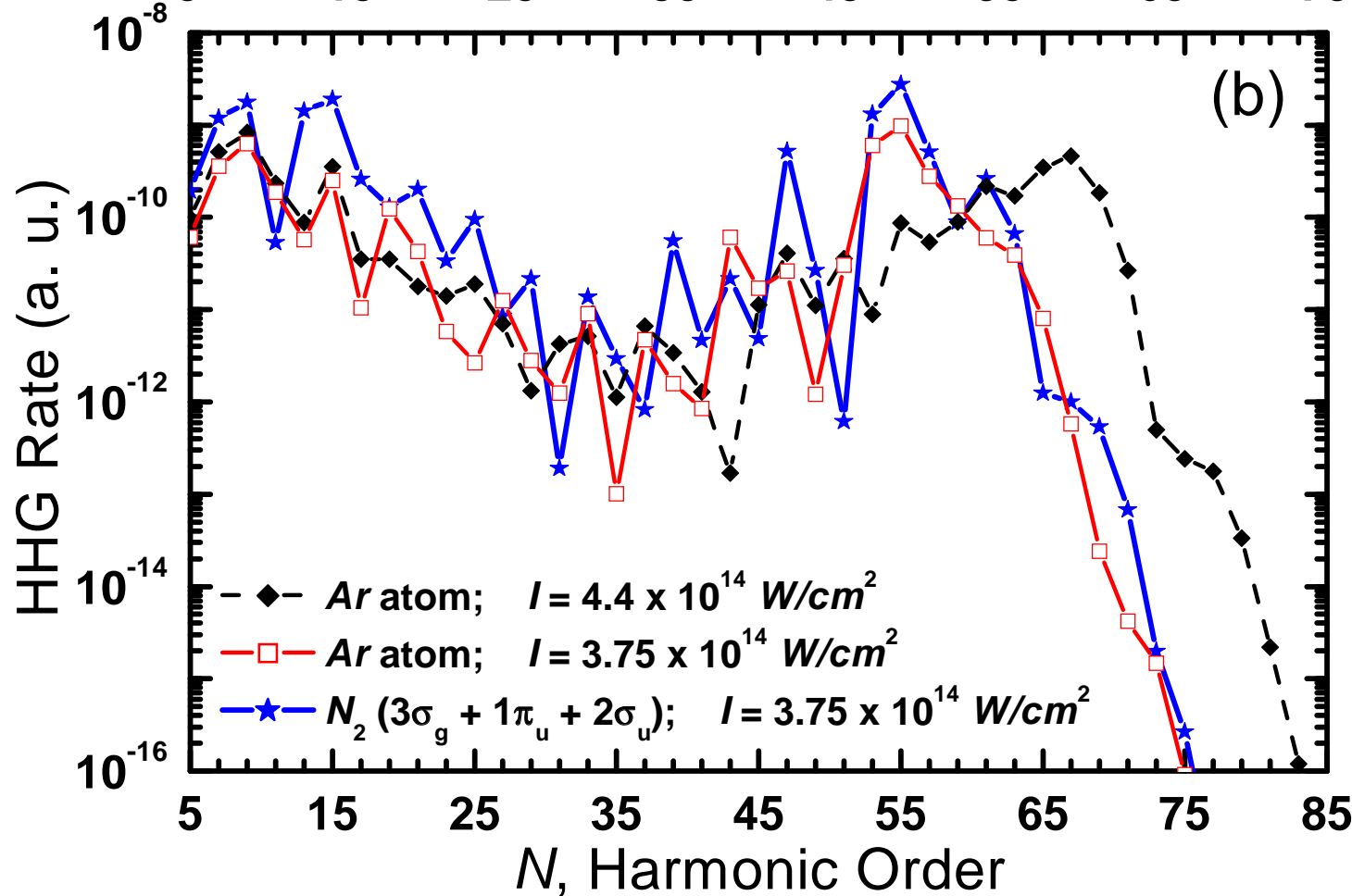
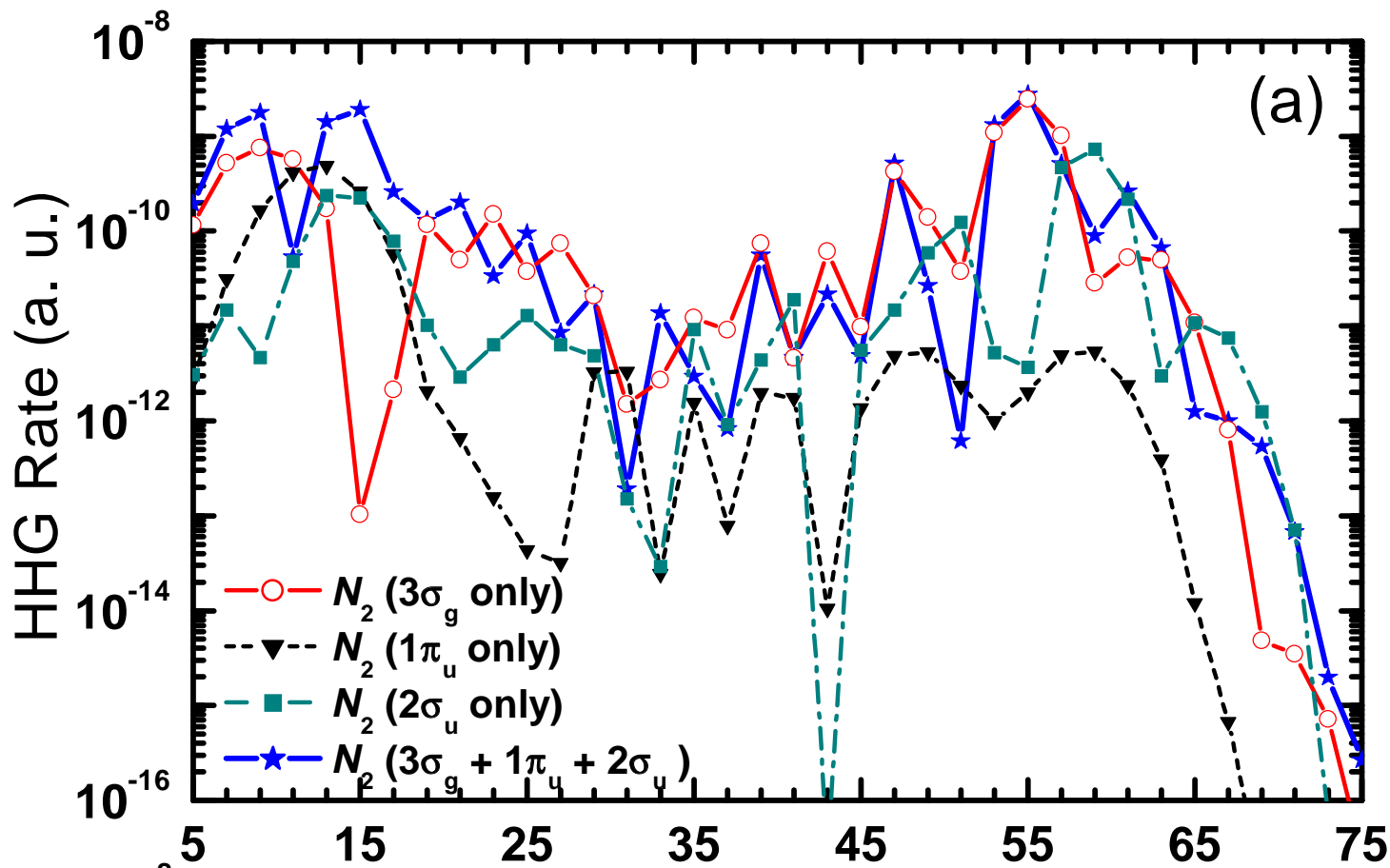


Fig. 6